



ELSEVIER

Available online at [www.sciencedirect.com](http://www.sciencedirect.com)

SCIENCE @ DIRECT®

International Journal of Multiphase Flow 30 (2004) 1279–1310

International Journal of  
**Multiphase  
Flow**

[www.elsevier.com/locate/ijmulflow](http://www.elsevier.com/locate/ijmulflow)

## Stability of a liquid jet into incompressible gases and liquids

T. Funada <sup>a</sup>, D.D. Joseph <sup>b,\*</sup>, S. Yamashita <sup>a</sup>

<sup>a</sup> Department of Digital Engineering, Numazu College of Technology, Ooka 3600, Numazu, Shizuoka 410-8501, Japan

<sup>b</sup> Department Aerospace Engineering and Mechanics, University of Minnesota, 110 Union Street,  
121 Akerman Hall, Minneapolis, MN 55455, USA

Received 21 May 2004; received in revised form 7 July 2004

### Abstract

We carry out an analysis of the stability of a liquid jet into a gas or another liquid using viscous potential flow. The instability may be driven by Kelvin–Helmholtz KH instability due to a velocity difference and a neckdown due to capillary instability. Viscous potential flow is the potential flow solution of Navier–Stokes equations; the viscosity enters at the interface.

KH instability is induced by a discontinuity of velocity at a gas–liquid interface. Such discontinuities cannot occur in the flow of viscous fluids. However, the effects of viscous extensional stresses can be obtained from a mathematically consistent analysis of the irrotational motion of a viscous fluid carried out here. An explicit dispersion relation is derived and analyzed for temporal and convective/absolute (C/A) instability. We find that for all values of the relevant parameters, there are wavenumbers for which the liquid jet is temporally unstable. The cut-off wavenumber and wavenumber of maximum growth are most important; the variation of these quantities with the density and viscosity ratios, the Weber number and Reynolds is computed and displayed as graphs and asymptotic formulas. The instabilities of a liquid jet are due to capillary and KH instabilities. We show that KH instability cannot occur in a vacuum but capillary instability can occur in vacuum. We present comprehensive results, based on viscous potential flow, of the effects of the ambient.

Temporally unstable liquid jet flows can be analyzed for spatial instabilities by C/A theory; they are either convectively unstable or absolutely unstable depending on the sign of the temporal growth rate at a singularity of the dispersion relation. The study of such singularities is greatly simplified by the analysis here which leads to an explicit dispersion relation; an algebraic function of a complex frequency and

\* Corresponding author. Tel.: +1 612 626 8000; fax: +1 612 626 1558.  
E-mail address: [joseph@aem.umn.edu](mailto:joseph@aem.umn.edu) (D.D. Joseph).

complex wavenumber. Analysis of this function gives rise to an accurate Weber–Reynolds criterion for the border between absolute and convective instabilities. Some problems of the applicability to physics of C/A analysis of stability of spatially uniform and nearly uniform flows are discussed.

© 2004 Elsevier Ltd. All rights reserved.

*Keywords:* Viscous potential flow; Kelvin–Helmholtz instability; Capillary instability; Temporal instability; Absolute and convective instability

---

## 1. Introduction

It is well known that the Navier–Stokes equations are satisfied by potential flow; the viscous term is identically zero when the vorticity is zero but the viscous stresses are not zero (Joseph and Liao, 1994). It is not possible to satisfy the no-slip condition at a solid boundary or the continuity of the tangential component of velocity and shear stress at a fluid–fluid boundary when the velocity is given by a potential. The viscous stresses enter into the viscous potential flow analysis of free surface problems through the normal stress balance at the interface.

Funada and Joseph (2002) constructed a viscous potential flow analysis of capillary instability of a liquid cylinder which was in excellent agreement with the exact fully viscous analysis. Funada and Joseph (2001) constructed a viscous potential flow analysis of Kelvin–Helmholtz instability in a channel. A fully viscous flow analysis is not available because the basic flow which postulates two uniform streams with different velocities is incompatible with, the requirement that the shear stress and tangential component of velocity should be continuous and the no-slip conditions at the channel wall. The analysis of Funada and Joseph (2001) is in much better agreement with experiments reviewed by Mata et al. (2002) than with other theories which account for the shear of the gas using different empirical correlations.

The excellent and well known book on stability theory by Drazin and Reid (1981) starts with an analysis of Rayleigh–Taylor, Kelvin–Helmholtz and capillary instability of an inviscid fluid. The potential flow analyses are not more difficult, but have a much richer content when the viscous contribution to the normal stress is not put to zero.

This paper is also allied to the analysis of temporal instability of the capillary jet given by Funada and Joseph (2002). Their analysis generalizes the inviscid analysis of Rayleigh (1878) in two ways: by accounting (i) for the viscosity of the jet and (ii) for the viscosity and density of the ambient media. The liquid jet is prey to capillary instability and Kelvin–Helmholtz instability due to the difference of the velocity of the jet and of the ambient media. The effects of discontinuous velocity can be obtained by a Galilean transformation to a fixed coordinate system relative to which the jet is moving with a velocity  $U$ . As a practical matter, the transformation  $z \rightarrow z + Ut$  transforms disturbances of the form  $\exp[i(kz - \omega t)]$  to  $\exp[i(kz - \tilde{\omega}t)]$  where  $\tilde{\omega} = \omega - kU$ . A Kelvin–Helmholtz instability due to velocity discontinuity cannot occur when the no-slip condition is applied.

In the present work we compute in a coordinate system fixed on the ambient fluid relative to which the jet velocity is  $U$ . We consider temporal, convective and absolute instability. The analysis of these instabilities is greatly simplified by viscous potential flow which leads to an explicit dispersion relation  $D(k, \omega) = 0$ , in which the ambient media with viscosity  $\mu_a$  and density  $\rho_a$  is

fully represented. Moreover, the analysis applies equally to jets into liquid and jet into gas;  $\rho_a$  and  $\mu_a$  stand for “air” for jets into air and for “ambient” for jets into liquid. This paper is organized so as to emphasize the case of jets into air which can be compared to the prior literature, which is reviewed below. The case of jets of viscous liquids into viscous liquids can be analyzed because viscous potential flow is consistent with a discontinuous velocity across the jet boundary.

The liquid jet is subject to Kelvin–Helmholtz instability due to the discontinuous velocity and to capillary instability due to surface tension. We show that Kelvin–Helmholtz instabilities cannot occur in a vacuum. The only other paper to treat the case of combined KH and capillary instability is that of Lin and Lian (1989) who analyzed the viscous problem using the Navier–Stokes equations but neglecting the effects of shear from the viscous gas. We call this type of solution “fully viscous flow (FVF)” in Section 10.

Other papers relevant to the stability of the liquid jet neglect viscosity altogether or neglect the effects of the ambient. Rayleigh’s (1878) study of temporal instability, the study of spatial instability of Keller et al. (1973), and Leib and Goldstein’s (1986a) study of C/A instability neglect viscosity and the effects of the ambient. Leib and Goldstein (1986b) and Le Dizès (1997) account for the jet viscosity but neglect the ambient. Many examples of transition from convective to absolute instability arising in the breakup of sheets and jets are presented in the monograph of Lin (2003). In particular, Lin has an interesting discussion of the relevance of this transition to the transition from dripping to jetting under gravity. The comparisons are suggestive but the agreement between C/A theory and experiments is not definitive.

## 2. Problem formulation

A long liquid cylinder of density  $\rho$ , viscosity  $\mu$ , and of mean radius  $a$  moves with a uniform axial velocity  $U$  relative to an ambient gas (air) of  $\rho_a, \mu_a$ . With a cylindrical frame  $(r, \theta, z)$  fixed on the gas, the liquid cylinder is put in the region of  $0 \leq r < a + \eta$  and  $-\infty < z < \infty$ , where  $\eta = \eta(z, t)$  is the varicose interface displacement. The governing Navier–Stokes equations and interface conditions for disturbances of the cylinder and gas are made dimensionless with the following scales:

$$[\text{length, velocity, time, pressure}] = \left[ 2a, U, \frac{2a}{U}, \rho U^2 \right]. \quad (2.1)$$

In terms of this normalization, we may define Weber number  $W$ , Reynolds number  $R$ , density ratio  $\ell$  and viscosity ratio  $m$ :

$$W = \frac{\gamma}{\rho 2a U^2}, \quad R = \frac{U 2a}{\nu}, \quad \ell = \frac{\rho_a}{\rho}, \quad m = \frac{\mu_a}{\mu}, \quad (2.2)$$

where  $\gamma$  is the surface tension coefficient,  $\nu = \mu/\rho$ ,  $\nu_a = \mu_a/\rho_a$  and  $m/\ell = \nu_a/\nu$ .

This problem is a combination of capillary instability and Kelvin–Helmholtz instability. When  $W = 0$  ( $\gamma = 0$ ) the instability is generated by the velocity difference. An interesting feature of this instability is that even though the density and viscosity of the gas is much smaller than the liquid, the dynamical effects of the gas cannot be neglected. The relevant physical quantity is the kinematic viscosity  $\nu = \mu/\rho$ ; Funada and Joseph (2001) found that the stability limit for viscous potential flow is nearly independent of the viscosity when  $\nu_\ell > \nu_a$  with a sensible dependence when

$v_\ell < v_a$ , for small viscosities, the opposite of what intuition would suggest. Essentially the same result holds for Kelvin–Helmholtz of liquid jet, studied here. The other limit  $W \rightarrow \infty$  or  $U \rightarrow 0$  leads to capillary instability which was studied using viscous potential flow, by Funada and Joseph (2002). Our sealing fails when  $U$  tends to zero; in the case the scale velocity is  $\gamma/\mu$  which is the characteristic velocity for capillary collapse and the relevant Reynolds number is  $J = \rho\gamma 2a/\mu^2$ . The basic flow in dimensionless coordinates is  $(\partial\Phi/\partial z, \partial\Phi_a/\partial z) = (1, 0)$  in terms of the velocity potential  $\Phi$  and  $\Phi_a$ .

For the liquid cylinder in a disturbed state ( $0 \leq r < 1/2 + \eta$  and  $-\infty < z < \infty$ ), the velocity potential  $\phi \equiv \phi(r, z, t)$  of an axisymmetric disturbance satisfies the Laplace equation:

$$\left(\frac{\partial^2}{\partial r^2} + \frac{1}{r} \frac{\partial}{\partial r} + \frac{\partial^2}{\partial z^2}\right)\phi = 0, \quad (2.3)$$

and the Bernoulli equation:

$$\frac{\partial\phi}{\partial t} + \frac{\partial\phi}{\partial z} + \frac{1}{2} \left(\frac{\partial\phi}{\partial r}\right)^2 + \frac{1}{2} \left(\frac{\partial\phi}{\partial z}\right)^2 + p = f(t), \quad (2.4)$$

where  $p \equiv p(r, z, t)$  is the pressure, and  $f(t)$  is an arbitrary function of time  $t$  which may be put to zero. For the gas disturbance of infinite extent ( $1/2 + \eta < r < \infty$  and  $-\infty < z < \infty$ ), the velocity potential  $\phi_a \equiv \phi_a(r, z, t)$  satisfies the equations:

$$\left(\frac{\partial^2}{\partial r^2} + \frac{1}{r} \frac{\partial}{\partial r} + \frac{\partial^2}{\partial z^2}\right)\phi_a = 0, \quad (2.5)$$

$$\ell \left[ \frac{\partial\phi_a}{\partial t} + \frac{1}{2} \left(\frac{\partial\phi_a}{\partial r}\right)^2 + \frac{1}{2} \left(\frac{\partial\phi_a}{\partial z}\right)^2 \right] + p_a = f_a(t). \quad (2.6)$$

The kinematic condition at the interface  $r = 1/2 + \eta$  is given for each fluid by

$$\frac{\partial\eta}{\partial t} + \frac{\partial\eta}{\partial z} + \frac{\partial\phi}{\partial z} \frac{\partial\eta}{\partial z} = \frac{\partial\phi}{\partial r}, \quad \frac{\partial\eta}{\partial t} + \frac{\partial\phi_a}{\partial z} \frac{\partial\eta}{\partial z} = \frac{\partial\phi_a}{\partial r}, \quad (2.7)$$

and the normal stress balance at  $r = 1/2 + \eta$  is given by

$$p - p_a - \frac{1}{R}\tau + \frac{m}{R}\tau_a = -W \left\{ \frac{\partial^2\eta}{\partial z^2} \left[ 1 + \left(\frac{\partial\eta}{\partial z}\right)^2 \right]^{-3/2} - (1/2 + \eta)^{-1} \left[ 1 + \left(\frac{\partial\eta}{\partial z}\right)^2 \right]^{-1/2} + 2 \right\}, \quad (2.8)$$

where the pressures at the interface are expressed by (2.4) and (2.6), and  $\tau$  and  $\tau_a$  denote the normal viscous stresses acting on the interface:

$$\tau = 2 \left[ \frac{\partial^2\phi}{\partial r^2} - 2 \frac{\partial^2\phi}{\partial r \partial z} \frac{\partial\eta}{\partial z} + \frac{\partial^2\phi}{\partial z^2} \left(\frac{\partial\eta}{\partial z}\right)^2 \right] \left[ 1 + \left(\frac{\partial\eta}{\partial z}\right)^2 \right]^{-1}, \quad (2.9)$$

$$\tau_a = 2 \left[ \frac{\partial^2 \phi_a}{\partial r^2} - 2 \frac{\partial^2 \phi_a}{\partial r \partial z} \frac{\partial \eta}{\partial z} + \frac{\partial^2 \phi_a}{\partial z^2} \left( \frac{\partial \eta}{\partial z} \right)^2 \right] \left[ 1 + \left( \frac{\partial \eta}{\partial z} \right)^2 \right]^{-1}, \tag{2.10}$$

For a case of the interface displacement small compared with the mean radius, (2.7)–(2.10) may be expanded around  $r = 1/2$  to give a linear system of boundary conditions for small disturbances. We do not require the continuity of tangential velocity and shear stress. The other conditions are that the liquid velocity is finite at the center  $r = 0$ , and the gas velocity should vanish as  $r \rightarrow \infty$ .

### 3. Dispersion relation

The potentials  $\phi$  and  $\phi_a$  are determined by (2.3) and (2.5). At the interface approximated by  $r = 1/2$ , the kinematic conditions are given by

$$\frac{\partial \eta}{\partial t} + \frac{\partial \eta}{\partial z} = \frac{\partial \phi}{\partial r}, \quad \frac{\partial \eta}{\partial t} = \frac{\partial \phi_a}{\partial r}, \tag{3.1}$$

and the normal stress balance is given by

$$-\left( \frac{\partial \phi}{\partial t} + \frac{\partial \phi}{\partial z} \right) + \ell \frac{\partial \phi_a}{\partial t} - \frac{2}{R} \frac{\partial^2 \phi}{\partial r^2} + \frac{2m}{R} \frac{\partial^2 \phi_a}{\partial r^2} = -W \left( \frac{\partial^2 \eta}{\partial z^2} + 4\eta \right). \tag{3.2}$$

Thus, we may have the solutions of the form

$$\eta = AE + \text{c.c.}, \quad \phi = A_1 I_0(kr)E + \text{c.c.}, \quad \phi_a = A_2 K_0(kr)E + \text{c.c.}, \tag{3.3}$$

where  $A$ ,  $A_1$  and  $A_2$  are the complex amplitudes,  $E \equiv \exp(ikz - i\omega t)$ ,  $\omega \equiv \omega_R + i\omega_I$  denotes the complex angular frequency,  $k \equiv k_R + ik_I$  the complex wavenumber,  $i = \sqrt{-1}$  and c.c. stands for the complex conjugate of the preceding expression;  $I_0(kr)$  and  $K_0(kr)$  denote the zeroth order of modified Bessel functions of the first and second kind. Then  $\phi$  gives the finite velocity at  $r = 0$  and  $\phi_a$  gives the velocity which vanishes as  $r \rightarrow \infty$ .

Substitution of (3.3) into (3.1) and (3.2) gives the dispersion relation,

$$D(k, \omega) = (\omega - k)^2 \alpha + \ell \omega^2 \alpha_a + i \frac{2k^2}{R} (\omega - k)b + i \frac{2mk^2}{R} \omega b_a - W(k^3 - 4k) = 0$$

which is a quadratic equation in  $\omega$

$$c_2 \omega^2 + 2c_1 \omega + c_0 = 0 \tag{3.4}$$

with the coefficients  $c_2 \equiv c_2(k)$ ,  $c_1 \equiv c_1(k)$  and  $c_0 \equiv c_0(k)$ ;

$$\left. \begin{aligned} c_2 &= \alpha + \ell \alpha_a, & c_1 &= -k\alpha + i \frac{k^2}{R} (b + mb_a) = c_{1R} + ic_{1I}, \\ c_0 &= k^2 \alpha - i \frac{2k^3}{R} b - W(k^3 - 4k) = c_{0R} + ic_{0I}, \end{aligned} \right\} \tag{3.5}$$

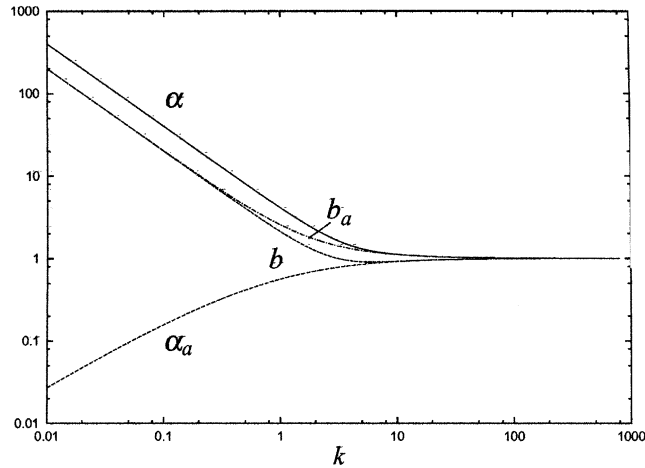


Fig. 1. Functions  $\alpha$ ,  $b_a$ ,  $b$  and  $\alpha_a$  versus real  $k$ ; these functions tend to one for  $k > 10$ . The neutral curves of inviscid and viscous potential flow for  $\ell = m$  are identical when  $k > 10$ ; this will be seen in (4.17). The functions for  $k > 10$  will lead to the asymptotic forms (4.7), (4.8) and (4.23)–(4.28), (4.28)–(4.30).

where  $\alpha$ ,  $\alpha_a$ ,  $b$  and  $b_a$  are defined as

$$\alpha = \frac{I_0(k/2)}{I_1(k/2)}, \quad \alpha_a = \frac{K_0(k/2)}{K_1(k/2)}, \quad b = \alpha - \frac{2}{k}, \quad b_a = \alpha_a + \frac{2}{k}. \tag{3.6}$$

It is noted for real  $k$  that  $k\alpha \rightarrow 4$  and  $\alpha_a \rightarrow 0$  as  $k \rightarrow 0$ , while  $\alpha \rightarrow 1$  and  $\alpha_a \rightarrow 1$  as  $k \rightarrow \infty$ ; this will be shown in Fig. 1. Apart from the Bessel functions, (3.4) is a cubic equation in  $k$ ; numerical calculations show that for each and every fixed set of parameters studied here, (3.4) gives rise to three complex roots.

#### 4. Temporal instability

For this case  $k$  is real and  $\omega = \omega_R + i\omega_I$ . Recalling that  $W = \gamma/(\rho 2aU^2)$ , we obtain pure KH instability with  $W = 0$ , and pure capillary instability with  $W \rightarrow \infty$ . A temporal growth rate curve is depicted as in Fig. 2, by which the maximum growth rate  $\omega_{Im}$ , the associated wavenumber  $k_m$  and the cut-off wavenumber  $k_c$  are defined.

##### 4.1. Inviscid fluids

When the fluids are both inviscid as  $R \rightarrow \infty$ , (3.4)–(3.6) reduce to

$$(\alpha + \ell\alpha_a)\omega^2 - 2k\alpha\omega + k^2\alpha - W(k^3 - 4k) = 0. \tag{4.1}$$

The complex angular frequency  $\omega = \omega_R + i\omega_I$  is given by

$$\omega_R = \frac{k\alpha}{\alpha + \ell\alpha_a}, \quad \omega_I = \pm \sqrt{\frac{k^2\ell\alpha\alpha_a}{(\alpha + \ell\alpha_a)^2} - \frac{W(k^3 - 4k)}{\alpha + \ell\alpha_a}} \tag{4.2}$$

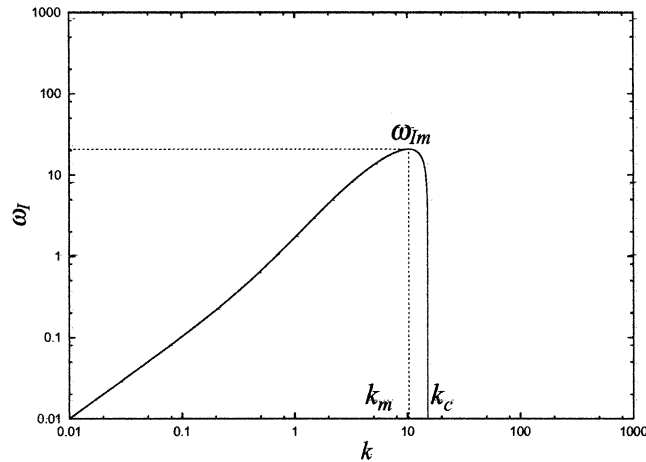


Fig. 2. Example of a growth rate curve defined in Section 4, showing the main features: the shape, maximum,  $\omega_{Im}$ ,  $k_m$  and the cut-off wavenumber  $k_c$ .

in the unstable case, and

$$\omega_R = \frac{k\alpha}{\alpha + \ell\alpha_a} \pm \sqrt{-\frac{k^2\ell\alpha\alpha_a}{(\alpha + \ell\alpha_a)^2} + \frac{W(k^3 - 4k)}{\alpha + \ell\alpha_a}}, \quad \omega_I = 0, \tag{4.3}$$

in the stable case. The neutral state is defined by  $\omega_I = 0$ ; either  $k = 0$  or  $W = W_c$  where

$$W_c^{-1} = \left[ \frac{\alpha + \ell\alpha_a}{\ell\alpha\alpha_a} \left( k - \frac{4}{k} \right) \right]_{k=k_c}. \tag{4.4}$$

Instability may arise in  $0 < k < k_c$ , where the *cut-off wavenumber*  $k_c$  ( $k_c \geq 2$  for which  $W_c^{-1} \geq 0$ ) is evaluated by (4.4) for given values of  $\ell$  and  $W_c$ . For  $k$  large for which  $\alpha$  and  $\alpha_a$  approach 1 (see Fig. 1), (4.4) is approximated as  $W_c^{-1} = (\ell^{-1} + 1)k_c$ .

The effects of surface tension, leading to capillary instability are absent when  $W = 0$ ; hence  $W = 0$  is pure KH instability. Inspection of (4.2) shows that *KH instability cannot occur when  $\ell = 0$* ; the viscosity and density of the ambient vanish so the *KH instability cannot occur in vacuum* (no pressure can be generated in vacuum). Pure KH instability is Hadamard unstable<sup>1</sup> with growth rate proportional to  $k$ ; the short waves grow exponentially with  $k$  at fixed  $t$ . The regularizing effect of surface tension is to stabilize short waves with  $k > k_c$  given by (4.4). The maximum growth rate

$$\omega_{Im} = \max_k \omega_I(k) = \omega_I(k_m) \tag{4.5}$$

<sup>1</sup> Hadamard instability is defined differently by different authors. For stability studies the growth rates  $\sigma(k)$  goes to infinity with  $k$ , the growth rates are not bounded for short waves. Say, for example  $\sigma = k$ ; the disturbance amplitude is proportional to  $\exp(kt)$ . This is a very bad instability; the amplitude tends to infinity with  $k$  for any fixed  $t$  no matter how small  $k$ ; the more you refine the mesh the worse is the result; they are very unstable to short waves. See Joseph (1990) and Joseph and Saut (1990).

may be obtained from (4.2) at an interior maximum for which

$$\partial\omega_I/\partial k = 0. \tag{4.6}$$

This computation is slightly complicated by that  $\alpha(k)$  and  $\alpha_a(k)$  depend on  $k$  weakly. The values  $\omega_{Im}$  and  $k_m$  depend on  $W$  and are plotted in Fig. 3. For large  $k$ ,  $\alpha(k) = \alpha_a(k) = 1$ , and we find that

$$\omega_{Im} = \frac{2\ell\sqrt{\ell}}{3\sqrt{3}(1+\ell)^2 W} \tag{4.7}$$

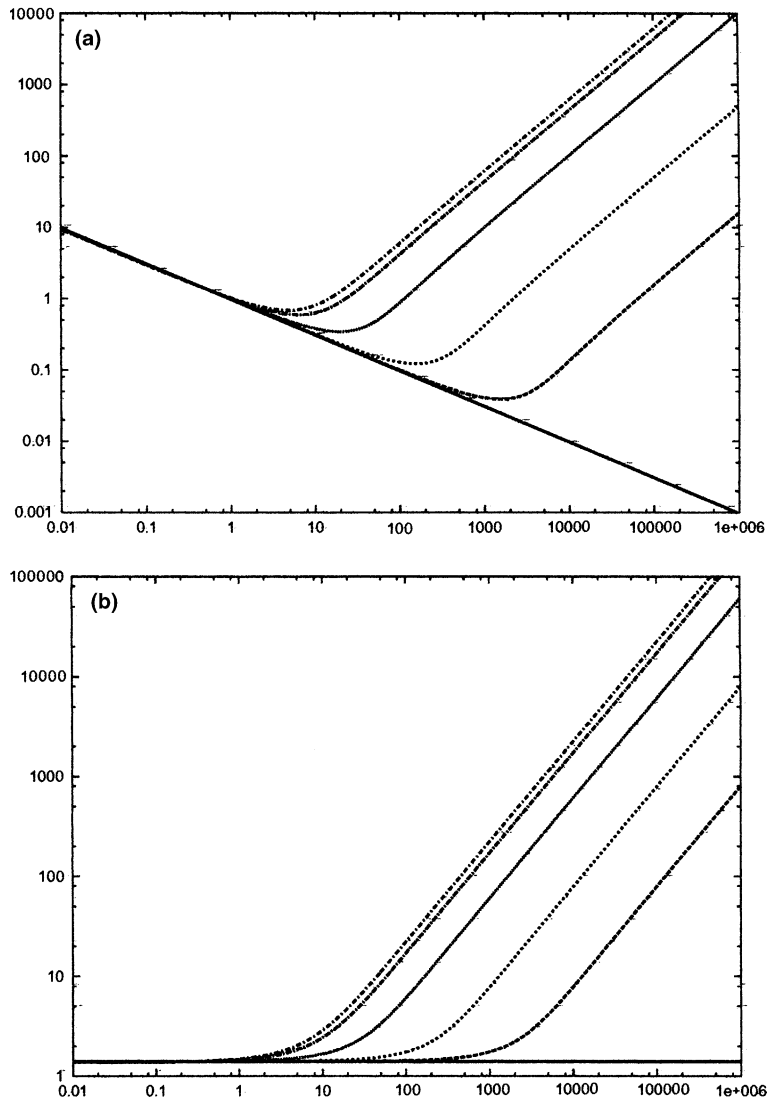


Fig. 3. (a)  $\omega_{Im}$  versus  $W^{-1}$  and (b)  $k_m$  versus  $W^{-1}$ , for  $\ell = 0$  (solid line), 0.0012 (broken line), 0.012 (dashed line), 0.1 (dotted line), 0.3455 (broken dotted line), 0.5 (dash dotted line). For large  $W^{-1}$  and  $\ell \neq 0$ , the curves approach the asymptotic form given respectively by (4.7) and (4.8).

and

$$k_m = \frac{2\ell}{3(1 + \ell)W}. \tag{4.8}$$

Eqs. (4.7) and (4.8) show that the maximum growth rate and the associated wavenumber tend to infinity for small  $W$  like  $1/W$ ; the wavelength  $\lambda_m = 2\pi/k_m$  tends to zero with  $W$ . Viscosity regularizes the growth rate but the wave length tends to zero with  $W$  as in the inviscid case (see Fig. 4).

For pure capillary instability with  $W \rightarrow \infty$ , the neutral boundaries are given by  $k = 0$  and  $k_c = 2$ . In this limiting case, we may rescale as  $\omega = \hat{\omega}\sqrt{W}$  by which (4.1) is expressed as

$$(\alpha + \ell\alpha_a)\omega^2 - W(k^3 - 4k) = 0 \quad \rightarrow \quad (\alpha + \ell\alpha_a)\hat{\omega}^2 - (k^3 - 4k) = 0, \tag{4.9}$$

so that the solution  $\hat{\omega}$  is given by

$$\hat{\omega} = \hat{\omega}_R + i\hat{\omega}_I = \pm \sqrt{\frac{k^3 - 4k}{\alpha + \ell\alpha_a}}; \tag{4.10}$$

hence instability ( $\hat{\omega} = i\hat{\omega}_I$ ) may arise in  $0 < k < 2$ . Disturbances with  $k > 2$  are stable and have an angular frequency  $\hat{\omega} = \hat{\omega}_R$ . The single column with  $\ell = 0$  is the case that Rayleigh analyzed in (1878).

#### 4.2. Viscous fluids

For  $\omega = \omega_R + i\omega_I$ , the quadratic equation (3.4) is separated into the real and imaginary parts

$$c_2(\omega_R^2 - \omega_I^2) + 2(c_{1R}\omega_R - c_{1I}\omega_I) + c_{0R} = 0, \tag{4.11}$$

$$2c_2\omega_R\omega_I + 2(c_{1R}\omega_I + c_{1I}\omega_R) + c_{0I} = 0 \quad \rightarrow \quad \omega_R = -\frac{2c_{1R}\omega_I + c_{0I}}{2c_2\omega_I + 2c_{1I}}, \tag{4.12}$$

to give the quartic equation in  $\omega_I$  alone:

$$a_4\omega_I^4 + a_3\omega_I^3 + a_2\omega_I^2 + a_1\omega_I + a_0 = 0, \tag{4.13}$$

with

$$\left. \begin{aligned} a_4 &= c_2^3, & a_3 &= 4c_2^3c_{1I}, & a_2 &= c_2c_{1R}^2 + 5c_2c_{1I}^2 - c_2^2c_{0R}, \\ a_1 &= 2c_{1R}^2c_{1I} + 2c_{1I}^3 - 2c_2c_{1I}c_{0R}, & a_0 &= c_{1R}c_{1I}c_{0I} - c_{1I}^2c_{0R} - \frac{1}{4}c_2c_{0I}^2. \end{aligned} \right\} \tag{4.14}$$

##### 4.2.1. Neutral curves

Neutral curves,  $\omega_I = 0$  in (4.13), are generated by the condition  $a_0 = 0$ :

$$a_0 = -\frac{k^6}{R^2}(m^2\alpha b_a^2 + \ell b^2\alpha_a) + \frac{k^4}{R^2}(b + mb_a)^2W(k^3 - 4k) = 0. \tag{4.15}$$

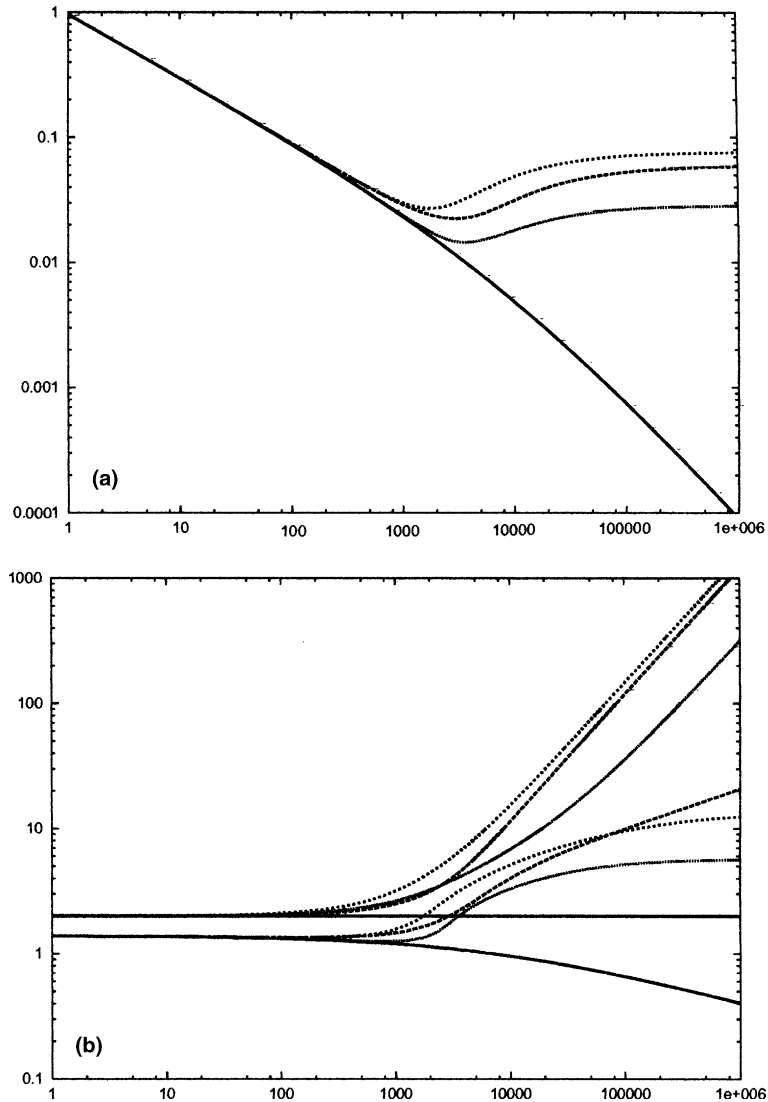


Fig. 4. (a)  $\omega_{Im}$  versus  $W^{-1}$  ( $=\rho 2aU^2/\gamma$ ) and (b)  $k_c$  (the upper curves) and  $k_m$  (the lower curves) versus  $W^{-1}$  for  $R = 100$ ; the solid curve is for  $\ell = 0$  and  $m = 0$ , the broken line for  $\ell = 0.0012$  and  $m = 0$ , the dashed line for  $\ell = 0.0012$  and  $m = 0.018$ , the dotted line for  $\ell = 0$  and  $m = 0.018$ . Kelvin–Helmholtz (KH) instability for the liquid jet corresponds to  $\gamma \rightarrow 0$  or  $W^{-1} \rightarrow \infty$ . The neutral curve is independent of the Reynolds number  $R$ . If surface tension and gravity are zero, KH flows are unstable for all  $k$  (see equation (2.27) in Funada and Joseph, 2001). When  $U \rightarrow 0$ , we get capillary instability which is unstable to all waves with  $0 < k < 2$ . The interval of unstable wave  $0 < k < k_c$  increases as the Weber number decreases (larger  $U$ , smaller  $\gamma$ ). In general, the neutral curve for viscous potential flow lies above that for inviscid potential flow with equality for a given  $k$  when  $m\alpha b_a = \ell b\alpha_a$  and for large  $k > 10$ , when  $\ell = m$ , ( $v = v_a$ ) (see Eqs. (4.20)–(4.22)). The values  $k_m(W^{-1})$  for which the growth is maximum depends on  $R$ . The maximum growth rates  $\omega_{Im}$  are finite for  $W \rightarrow 0$  but the associated wavenumbers are proportional to  $1/W$  for small  $W$ .

One root of (4.15) is  $k = 0$  and it is the only root when  $W = 0$  (Kelvin–Helmholtz instability). The other roots are given by

$$W^{-1} = \frac{(b + mb_a)^2}{m^2\alpha b_a^2 + \ell b^2\alpha_a} \left( k - \frac{4}{k} \right), \tag{4.16}$$

which has the general form shown in Fig. 4. Eqs. (4.13) and (4.15) show that when  $\ell = 0, m = 0$ , the only instability is due to capillarity *KH instability is not possible in vacuum*. An identical conclusion for KH instability of stratified gas–liquid flow in a horizontal rectangular channel follows from Eq. (3.4) in the paper by Funada and Joseph (2001). For large values of  $k, b, b_a, \alpha$  and  $\alpha_a$  tend to 1 and (4.16) reduces to

$$W^{-1} = \frac{(1 + m)^2}{m^2 + \ell} k. \tag{4.17}$$

When  $\ell = m$  ( $v = v_a$ ), this reduces to  $(\ell + 1)k/\ell$ , which is the same as the inviscid case given by (4.4).

A striking conclusion which follows from (4.15) and (4.16) is that the cut-off wavenumber  $k = k_c$  satisfying (4.16) is independent of the Reynolds number  $R$ ; when  $k > k_c$ , the liquid jet is stable.

A further comparison, (4.16) and (4.4), of inviscid and viscous potential flow shows that the neutral curves are identical under the condition that  $m\alpha b_a = \ell b\alpha_a$ . Fig. 1 shows that  $\alpha b_a = b\alpha_a$  for  $k > 10$ ; in this case the neutral curves are identical when  $\ell = m$  (or  $v = v_a$ ). It is of interest that for jets of liquid into air  $\ell \ll 1$  and  $m \ll 1$ . In this limit both (4.16) and (4.4) reduce to

$$W^{-1} = \frac{1}{\ell\alpha_a} \left( k - \frac{4}{k} \right). \tag{4.18}$$

This surprising and anti-intuitive result says that the neutral condition for a highly viscous liquid  $m \rightarrow 0$  is the same as for two inviscid fluids provided that  $\ell \ll 1$ .

The ratio (4.16)/(4.4) may be written as

$$\frac{W_{VPF}^{-1}}{W_{IPF}^{-1}} = \frac{(b + mb_a)^2 \ell \alpha \alpha_a}{(m^2 \alpha b_a^2 + \ell b^2 \alpha_a)(\alpha + \ell \alpha_a)} \tag{4.19}$$

where VPF and IPF stand for viscous and inviscid potential flow. For large  $k > 10$ , this reduces to

$$\frac{W_{VPF}^{-1}}{W_{IPF}^{-1}} = \frac{(1 + m)^2 \ell}{(m^2 + \ell)(1 + \ell)}. \tag{4.20}$$

For  $m = 0$  (the viscosity of the jet is much larger than the ambient)

$$\frac{W_{VPF}^{-1}}{W_{IPF}^{-1}} = \frac{1}{1 + \ell} \leq 1. \tag{4.21}$$

For  $m \rightarrow \infty$  (the viscosity of the jet is much smaller than the ambient)

$$\frac{W_{VPF}^{-1}}{W_{IPF}^{-1}} = \frac{\ell}{1 + \ell} \leq 1. \tag{4.22}$$

In general, the neutral curve for viscous potential flow is below (or at least not above) that of inviscid potential flow.

For all values of  $\ell$ ,  $R$  and  $W$ , there are wavenumbers for which  $\omega_I > 0$ ; the liquid jet is always unstable to temporal disturbances in analysis based on viscous potential flow.

#### 4.2.2. Growth rate curves

An example of a growth rate curve is shown as Fig. 2. All of the growth rate curves have this same form and may be characterized by three parameters: the maximum growth rate  $\omega_{Im}$  and wavenumber  $k_m$ ,  $\omega_{Im} = \omega_I(k_m)$  and the cut-off wavenumber  $k_c$ , as shown in Fig. 2.  $\omega_{Im}$  and  $k_m$  depend on  $R$ , but  $k_c$  is independent of  $R$ .

The variation of  $\omega_{Im}$  and  $k_m$  with  $W^{-1}$  is shown in Fig. 4. The effect of viscosity is to regularize the Hadamard instability,  $\omega_{Im}$  tends to a finite value as  $W \rightarrow \infty$  (cf, Figs. 4 and 5). For large values of  $W^{-1}$ , KH instability dominates. The great difference between stability in vacuum  $(\ell, m) = (0, 0)$  and inviscid gas  $m = 0$ ,  $\ell \neq 0$  is apparent for large values of  $W^{-1}$ .

For large  $k$  ( $> 10$ ) for which  $\alpha = \alpha_a = b = b_a = 1$ , the imaginary part of the dispersion relation (4.12) gives  $\omega_R$ :

$$\omega_R = \frac{k\omega_I + \frac{k^3}{R}}{(1 + \ell)\omega_I + \frac{k^2}{R}(1 + m)} = \frac{k}{(1 + \ell)X} \left[ X + \frac{k^2}{R}(\ell - m) \right], \quad (4.23)$$

where  $X$  is defined as

$$X = (1 + \ell)\omega_I + \frac{k^2}{R}(1 + m). \quad (4.24)$$

The real part of the dispersion relation (4.11) leads to the quadratic equation of  $X^2$ :

$$\frac{k^2}{X^2} \frac{k^4}{R^2} (\ell - m)^2 - X^2 + 2Y = 0, \quad (4.25)$$

with

$$Y = \frac{1}{2} \left[ \frac{k^4}{R^2} (1 + m)^2 + \ell k^2 - (1 + \ell)W(k^3 - 4k) \right], \quad (4.26)$$

whence the solution to (4.25) is expressed as

$$X = (1 + \ell)\omega_I + \frac{k^2}{R}(1 + m) = \left[ Y + \sqrt{Y^2 + \frac{k^6}{R^2}(\ell - m)^2} \right]^{1/2}, \quad (4.27)$$

When  $\ell = m$ , the solution (4.27) reduces to

$$X = (1 + \ell)\omega_I + \frac{k^2}{R}(1 + m) = \sqrt{2Y}. \quad (4.28)$$

When  $R \rightarrow \infty$ , the solution (4.27) reduces to the inviscid case:

$$X = (1 + \ell)\omega_I = [\ell k^2 - (1 + \ell)W(k^3 - 4k)]^{1/2}. \quad (4.29)$$

The solution (4.27) is available to have the maximum growth rate and the cut-off wavenumber when those exist in large  $k$  under the condition that  $\ell \neq 0$  or  $m \neq 0$ , for which  $W^{-1}$  is large.

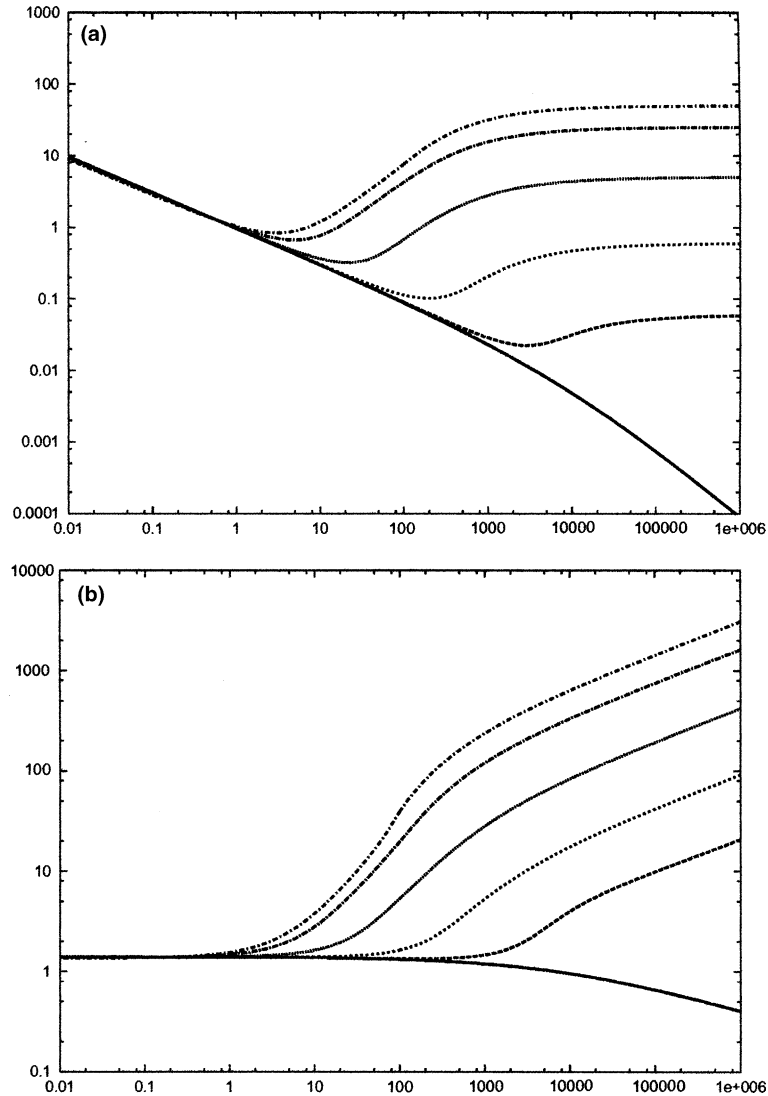


Fig. 5. (a)  $\omega_{Im}$  versus  $W^{-1}$  and (b)  $k_m$  versus  $W^{-1}$  for  $R = 100$ ,  $m = 0$  and various  $\ell$ ;  $\ell = 0$  (solid line), 0.0012 (broken line), 0.012 (dashed line), 0.1 (dotted line), 0.5 (broken dotted line), 1 (dash dotted line). For large  $W^{-1}$  and  $\ell \neq 0$ , the curves approach the asymptotic form given by (4.30).

The extremum value of  $\omega_I$  is given by differentiating (4.27) and imposing  $\partial\omega_I/\partial k = 0$  at  $k = k_m$ :

$$\omega_{Im} = -\frac{k_m^2}{R} \frac{(1+m)}{(1+\ell)} + \frac{R/(1+m)}{4k_m(1+\ell)} \left\{ \frac{\partial Y}{\partial k} + \left[ Y \frac{\partial Y}{\partial k} + \frac{3k^5}{R^2} (\ell - m)^2 \right] \left[ Y^2 + \frac{k^6}{R^2} (\ell - m)^2 \right]^{-1/2} \right\}_{k=k_m} \quad (4.30)$$

The expression for  $k_m$  is rather cumbersome; it shows that  $k_m \propto 1/W$  for small  $W$  even though  $\omega_I(k_m)$  is bounded as  $W \rightarrow 0$  (Figs. 4 and 5). It follows that the wave length  $\lambda_m = 2\pi/k_m$  tends

to zero with  $W$ . If this KH disturbance leads to breakup, we would find small liquid fragments even to fine mist.

4.3. Nonaxisymmetric disturbances

The authors of papers on spatial, temporal and C/A theory cited at the end of Section 1 restrict the attention to axisymmetric disturbances. Yang (1992) studied the stability of an inviscid liquid jet to axisymmetric and nonaxisymmetric temporal disturbances. He found wavenumber ranges

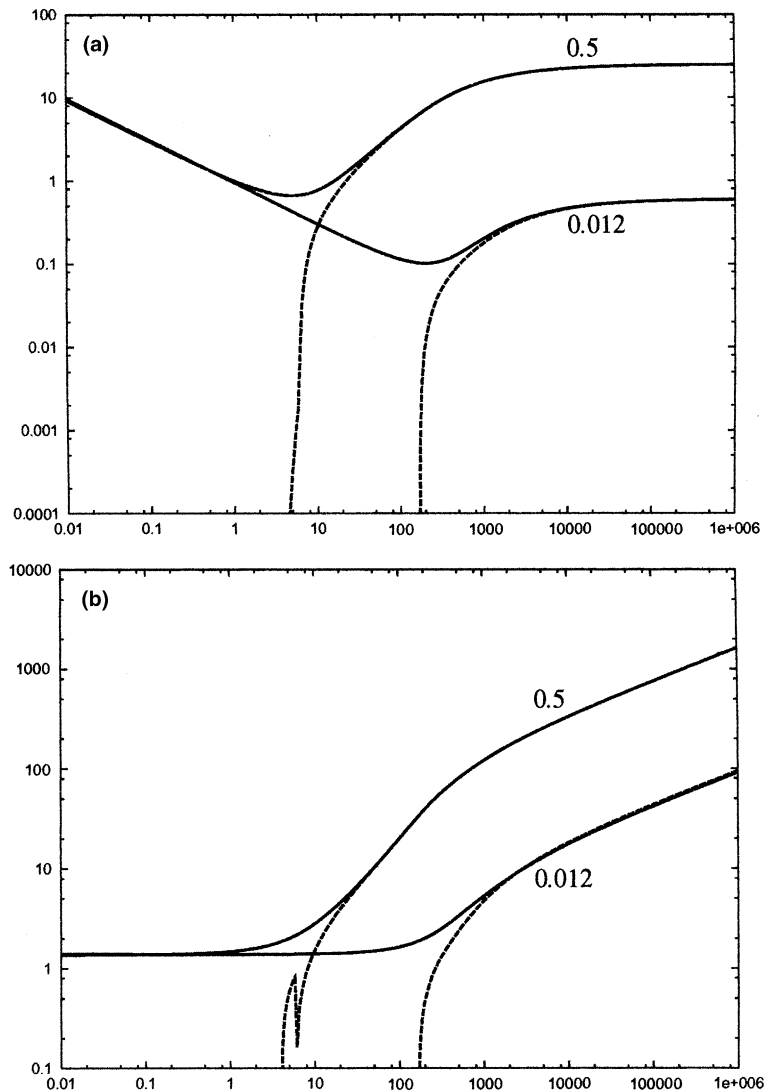


Fig. 6. (a)  $\omega_{Im}$  versus  $W^{-1}$  and (b)  $k_m$  versus  $W^1$  for  $R = 100$ , and  $m = 0$ ;  $\ell = 0.012$  and  $n = 0$  (solid line),  $\ell = 0.012$  and  $n = 1$  (broken line),  $\ell = 0.5$  and  $n = 0$  (solid line),  $\ell = 0.5$  and  $n = 1$  (broken line).

for which the nonaxisymmetric disturbances grow faster, but the greatest peak values of  $\omega_1(k_m)$  are for axisymmetric disturbances. A preliminary study of axisymmetric disturbances proportional to  $\exp(in\theta)$  with  $n = 0$  and asymmetric disturbances with  $n > 0$ , especially with  $n = 1$  yielded results similar to those found by Yang (1992) for the inviscid jet. The peak growth rates are always attained for  $n = 0$  in flows with capillary numbers  $W$  larger than small value, say 1/10; for KH instability  $W \rightarrow \infty$ , the peak values for  $n = 0$  and  $n = 1$  are nearly identical (see Fig. 6).

Li and Kelly (1992) did an analysis of an inviscid liquid jet in a compressible high speed air-stream. They found that  $n = 1$  is the most dangerous mode when the Mach number is near to one. The case of nonaxisymmetric disturbances needs further study.

### 5. Numerical results of temporal instability

Here we present neutral curves and growth rates for the stability of viscous liquids into air comparing viscous potential flow (VPF) with inviscid potential flow (IPF).

Using the data of Funada and Joseph (2002), various liquid–gas cases are shown in Table 1. The parameters of the growth rate curves for the 10 cases are defined in Fig. 2 and given in Table 2 for typical values of  $U$ . The neutral curves  $W^{-1}(k)$  for all 10 cases start at  $k = 2$ . For large  $k$  ( $>10$ ), they may be computed exactly from (4.17) and compared with inviscid potential flow using (4.20). The differences between viscous and inviscid potential flow vanish for  $k > 10$  when  $m\alpha\omega b_a = lb\alpha_a$  and for all  $k$  when  $\rho_a \ll \rho$ ,  $\mu_a \ll \mu$  when  $\mu$  is very large, as shown previously.

### 6. Spatial, absolute and convective instability

The motivation for considering spatial instability of a liquid jet was very clearly expressed by Keller et al. (1973) who noted that the disturbance initiating from the nozzle tip actually grows in space as it is swept downstream, where it is observed to break into drops, leaving a section of jet intact near the nozzle tip as would occur for a disturbance that is convectively unstable. Such disturbances proportional to  $\exp(ikz - i\omega t)$  can be described by allowing  $k$  to be complex and  $\omega$  real

Table 1  
Data of various liquid–gas cases

No.	Liquid Cylinder–gas	$\ell = \rho_a/\rho$	$m = \mu_a/\mu$	$m/\ell = \nu_a/\nu$	$\sqrt{\gamma/(\rho 2a)}$ (m/s)
1	Mercury–air	8.889E–05	1.154E–02	1.298E+02	5.976E–02
2	Water–air	1.200E–03	1.800E–02	1.500E+01	8.532E–02
3	Benzene–air	1.395E–03	2.769E–02	1.985E+01	5.793E–02
4	SO100–air	1.238E–03	1.800E–04	1.454E–01	4.655E–02
5	Glycerine–air	9.547E–04	2.302E–05	2.411E–02	7.102E–02
6	Oil–air	1.478E–03	3.830E–05	2.592E–02	5.984E–02
7	SO10000–air	1.238E–03	1.800E–06	1.454E–03	4.655E–02
8	SO10–air	1.238E–03	1.800E–03	1.454E+00	4.655E–02
9	Silicon oil–nitrogen	1.345E–03	8.750E–04	6.508E–01	4.697E–02
10	Silicon oil–nitrogen	1.326E–03	1.750E–03	1.319E+00	4.620E–02

Table 2

Parameters of the growth rate curves identified in Fig. 2 for the 10 cases of liquid–gas flow in Table 1

No.	$U$ (m/s)	$W$	$W^{-1}$	$R$	$\omega_{Im}^{VPF}$	$k_m^{VPF}$	$k_c^{VPF}$	$\omega_{Im}^{VPF}$	$k_m^{IPF}$	$k_c^{IPF}$
1	0.02	8.928	0.112	0.17308E+04	0.9709	1.394	2.000	0.9711	1.394	2.000
	0.06	0.992	1.008	0.51923E+04	0.9709	1.394	2.000	0.9711	1.394	2.000
	0.10	0.357	2.800	0.86538E+04	0.9709	1.394	2.000	0.9712	1.394	2.000
2	0.02	18.200	0.055	0.20000E+03	0.9698	1.393	2.000	0.9710	1.394	2.000
	0.06	2.022	0.495	0.60000E+03	0.9699	1.393	2.000	0.9711	1.394	2.000
	0.10	0.728	1.374	0.10000E+04	0.9701	1.394	2.000	0.9713	1.394	2.000
3	0.02	8.390	0.119	0.26462E+03	0.9696	1.393	2.000	0.9710	1.394	2.000
	0.06	0.932	1.073	0.79385E+03	0.9699	1.394	2.000	0.9713	1.394	2.000
	0.10	0.336	2.980	0.13231E+04	0.9704	1.394	2.001	0.9718	1.395	2.001
4	0.02	5.418	0.185	0.19380E+01	0.7890	1.244	2.000	0.9710	1.394	2.000
	0.06	0.602	1.661	0.58140E+01	0.7893	1.244	2.000	0.9714	1.395	2.000
	0.10	0.217	4.614	0.96900E+01	0.7898	1.245	2.001	0.9722	1.396	2.001
5	0.02	12.609	0.079	0.32148E+00	0.5138	0.988	2.000	0.9710	1.394	2.000
	0.06	1.401	0.714	0.96445E+00	0.5139	0.988	2.000	0.9712	1.394	2.000
	0.10	0.504	1.983	0.16074E+01	0.5140	0.988	2.000	0.9714	1.395	2.000
6	0.02	8.951	0.112	0.36431E+00	0.5028	0.977	2.000	0.9710	1.395	2.000
	0.06	0.995	1.005	0.10929E+01	0.5029	0.977	2.000	0.9713	1.395	2.000
	0.10	0.358	2.793	0.18215E+01	0.5031	0.977	2.001	0.9718	1.396	2.001
7	0.02	5.418	0.185	0.19380E-01	0.0430	0.278	2.000	0.9710	1.394	2.000
	0.06	0.602	1.661	0.58140E-01	0.0430	0.279	2.000	0.9714	1.395	2.000
	0.10	0.217	4.614	0.96900E-01	0.0430	0.278	2.002	0.9722	1.396	2.001
8	0.02	5.418	0.185	0.19380E+02	0.9488	1.376	2.000	0.9710	1.394	2.000
	0.06	0.602	1.661	0.58140E+02	0.9492	1.377	2.000	0.9714	1.395	2.000
	0.10	0.217	4.614	0.96900E+02	0.9499	1.378	2.002	0.9722	1.396	2.001
9	0.02	5.515	0.181	0.95200E+01	0.9273	1.359	2.000	0.9710	1.394	2.000
	0.06	0.613	1.632	0.28560E+02	0.9277	1.359	2.000	0.9714	1.395	2.000
	0.10	0.221	4.533	0.47600E+02	0.9284	1.361	2.002	0.9722	1.396	2.002
10	0.02	5.337	0.187	0.19300E+02	0.9485	1.376	2.000	0.9710	1.394	2.000
	0.06	0.593	1.686	0.57900E+02	0.9489	1.377	2.000	0.9714	1.395	2.000
	0.10	0.213	4.684	0.96500E+02	0.9497	1.378	2.002	0.9723	1.396	2.002

Viscous (VPF) and (IPF) are compared.

so that disturbances can grow in space but not in time. They found that Rayleigh's results are relevant only when the Weber number  $W = \gamma/(\rho 2aU^2)$  is small and the spatial growth rate  $k_I$  is related to the temporal growth rate  $\omega_I$  by the relation  $k_I = \pm\omega_I + O(W)$ , while the disturbance travels at the jet velocity. For large values of  $W$ , they found a new mode of faster growing disturbances whose wavelengths are perhaps too long to be observable.

Leib and Goldstein (1986b) showed that the new mode corresponds to an absolute instability which arises from a pinch point singularity in the dispersion relation. An absolutely unstable wave packet propagates upstream and downstream and hence such disturbances spread over the whole

$z$  domain of flow; the flow is unstable at any  $z$ , as  $t$  increases. This is not the picture advanced by Keller et al. (1973) in which the region close to the discharge is never corrupted by growing disturbances.

One of the aims of the theory of absolute and convective instability is to provide a frame for the problem of spatial development of disturbances. The spatial development of controlled disturbances such as are generated by a vibrating ribbon at the start of a growing boundary layer or at the inlet of a plane Poiseuille flow calculated from spatial theory yielded good results with experiments in which disturbances were suppressed. However the spatial theory has no rigorous foundation; for example, a spatial mode, when it can be defined, is inadmissible when it is unbounded at infinity, though it may describe the spatial evolution of disturbances of a given frequency for a long time (see Drazin and Reid, 1981 section 32 for experiments; section 47.1 for theoretical problems).

To deal with the problem of propagation of impulses, the concept of convective and absolutely unstable solutions (C/A for short) has been introduced. The definitions of instability in the C/A context is formulated in terms of the evolution of impulses at the origin in the  $(x, t)$  plane proportional initially to the product  $\delta(x)\delta(t)$ . A flow is called *linearly stable* if this disturbance decays to zero along all rays  $x/t = \text{const}$ . It is *linearly unstable* if the impulse tends to infinity along at least one ray  $x/t = \text{const}$ . An unstable flow is *linearly convectively unstable* if the impulse tends to zero along the ray  $x/t = 0$  and is *absolutely unstable* if the impulse tends to infinity along the ray  $x/t = 0$ . Obviously an absolutely unstable impulse is linearly unstable.

A cartoon for wave packets propagating from the origin in these four cases is shown in Fig. 7. The C/A concepts are not straightforward and need explanation. Huerre (2000) notes that

A parallel shear flow of given velocity profile is said to be *convectively unstable* if the growing wavepacket produced in response to an impulsive source localized in space and time is advected away. It is *absolutely unstable* if the growing wavepacket expands around the source to contaminate the entire medium. In the case of parallel flows that are invariant under Galilean transformations, this distinction appears at first sight to be preposterous: a simple change of reference frame transforms a flow from convectively unstable to absolutely unstable and vice versa, and the ‘laboratory frame’ is not properly defined. However, when Galilean invariance is broken, e.g. in spatially developing flows, in flows with a definite origin, or in flows forced at a specific streamwise station, the laboratory frame is singled

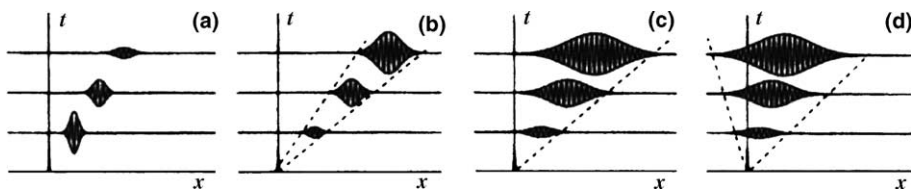


Fig. 7. Linear impulse response. (a) Linearly stable flow; (b) linearly convectively unstable flow; (c) marginally convectively/absolutely unstable flow; (d) absolutely unstable flow (after Huerre, 2000, Fig. 8). The pictures here are for a response to a linear impulses; stability cannot be determined from the evolution of impulses alone. Convectively unstable flows in (b) are also temporally unstable; at any  $x$ , real wavenumbers exist for which disturbances outside the unstable wedge in (b) will grow.

out and it is precisely in these instances that the distinction between convective and absolute instability becomes of interest. It should be emphasized that, in order for these concepts to be relevant, one must enforce a *scale-separation* assumption: the flow under consideration must be slowly evolving along the stream over a typical instability wavelength. This strong hypothesis is made throughout the ensuing theoretical developments in order to recover the locally parallel flow instability properties as a leading-order approximation at each streamwise station.

Parallel flows which are temporally stable are also stable in the C/A theory. Temporally unstable flows can be absolutely or convectively unstable. Disturbances from a source, like a vibrating ribbon, can propagate without corrupting the source, only if the flow is convectively unstable and only if random disturbances at fixed points which are temporally unstable are suppressed.

In this paper we follow others in considering the open basic flow which has no spatial variation in the axial direction which is Galilean invariant. The point of novelty of our analyses is that the stability analysis is carried out using the equations of viscous potential flow which allow a discontinuous velocity at the jet surface but accommodates effects of viscosity, viscosity ratios, density ratios, etc. but still leads to an explicit dispersion relation.

Huerre and Monkewitz (1985) point out that the spatial stability theory is applicable when the flow is convectively unstable and not when the flow is absolutely unstable. They describe a methodology based on Bers (1975) criterion, to determine when a free shear layer is convectively unstable. Their problem is difficult and does not give rise to an explicit dispersion; numerical computations are required. The search for the border between absolute and convective instability is a function of prescribed parameters and requires knowledge of the dispersion relation for complex frequencies and wavenumbers. This search is greatly simplified in the case of the stability of the liquid jet based on viscous potential flow because the search for singularities of the dispersion relation is reduced to the study of algebraic equations of two complex variables.

We use the criterion of Bers (1975) which says that an unstable flow is convectively unstable if the modes proportional to  $\exp(ikz - i\omega t)$  of complex frequency  $\omega$  and  $k$ , which have a zero group velocity

$$G_V = \partial\omega_R/\partial k_R = 0, \quad (6.1)$$

are all temporally damped,  $\omega_I < 0$ . Otherwise the system is absolutely unstable. If  $\omega_R$  does not change with  $k_R$  and  $\omega_I < 0$ , then a disturbance with excitation frequency  $\omega_R$  will decay in time but can grow in space. On the other hand, we do not use the method of Briggs (1964) and Bers (1975). Instead, we implement an algebraic study of the dispersion relation.

Following Schmid and Henningson (2001), we may characterize the singularities of  $D(k, \omega)$  at  $k_0, \omega_0$  by the equation

$$D(k_0, \omega_0) = 0, \quad \frac{\partial D}{\partial k}(k_0, \omega_0) = 0, \quad \frac{\partial^2 D}{\partial k^2}(k_0, \omega_0) \neq 0. \quad (6.2)$$

In the neighborhood of  $k_0, \omega_0$  a Taylor series expansion of  $D(k, \omega)$  leads to

$$0 = \frac{\partial D}{\partial \omega} \Big|_0 (\omega - \omega_0) + \frac{1}{2} \frac{\partial^2 D}{\partial k^2} \Big|_0 (k - k_0)^2 + HO \quad (6.3)$$

where  $HO$  are terms that go to zero faster than the terms retained. This results in a square root singularity for the local map between the  $k$  and  $\omega$  planes.

If we imagine  $D(k, \omega) = 0$  to be solved for  $\omega = \omega(k)$ , then  $D(k, \omega(k)) = 0$  is an identity in  $k$  and

$$0 = \frac{dD}{dk} = \frac{\partial D}{\partial k} + \frac{\partial \omega}{\partial k} \frac{\partial D}{\partial \omega} \tag{6.4}$$

and

$$\hat{c} \equiv \frac{\partial \omega}{\partial k} = - \frac{\partial D}{\partial k} / \frac{\partial D}{\partial \omega} = \hat{c}_R + i\hat{c}_I \tag{6.5}$$

can be said to be a complex-valued “generalized” group velocity which must be zero at the singularity. This is not the ordinary group velocity. If  $\partial D/\partial \omega \neq 0$ , and it is not equal to zero in this study, then

$$\hat{c} = \frac{\partial \omega}{\partial k} = 0 \quad \text{when} \quad \frac{\partial D}{\partial k} = 0. \tag{6.6}$$

Moreover,

$$\frac{\partial \omega}{\partial k} = \frac{1}{2} \left( \frac{\partial \omega_R}{\partial k_R} + \frac{\partial \omega_I}{\partial k_I} \right) + \frac{i}{2} \left( \frac{\partial \omega_I}{\partial k_R} - \frac{\partial \omega_R}{\partial k_I} \right) \tag{6.7}$$

and  $\hat{c} = 0$  does not imply that the group velocity  $G_V = \partial \omega_R / \partial k_R = 0$ . However, since the Cauchy–Riemann condition for a function  $\omega(k)$  holds, then  $\partial \omega / \partial \bar{k} = 0$  and

$$\frac{\partial \omega_R}{\partial k_R} = \frac{\partial \omega_I}{\partial k_I}, \quad \frac{\partial \omega_I}{\partial k_R} = - \frac{\partial \omega_R}{\partial k_I}. \tag{6.8}$$

Hence, if (6.6) holds, then (6.8) implies that

$$G_V = \frac{\partial \omega_R}{\partial k_R} = \frac{\partial \omega_I}{\partial k_I} = 0 \quad \text{and} \quad \frac{\partial \omega_R}{\partial k_I} = - \frac{\partial \omega_I}{\partial k_R} = 0. \tag{6.9}$$

### 7. Algebraic equations at a singular point

A *singular point* satisfies (6.2); alternatively,  $D = \hat{c} = 0$ . These are complex equations, four real equations for  $k_R, k_I, \omega_R$  and  $\omega_I$  when the other parameters are prescribed. If  $\omega_I < 0$  at a singular point the flow is convectively unstable. A *critical singular point* is a singular point such that  $\omega_I = 0$ .

For given values of the parameters ( $\ell, W, R$  and  $m = 0$ ), the solution  $k = k_R + ik_I$  ( $\omega(k) = \omega_R + i\omega_I$ ) of the dispersion relation (3.4)–(3.6) is obtained implicitly. Eq. (3.4) is a quadratic in  $\omega$  and has two roots,  $\omega_1$  and  $\omega_2$ :

$$\omega_1 = -\frac{c_1}{c_2} + \sqrt{\left(\frac{c_1}{c_2}\right)^2 - \frac{c_0}{c_2}}, \quad \omega_2 \equiv \omega = -\frac{c_1}{c_2} - \sqrt{\left(\frac{c_1}{c_2}\right)^2 - \frac{c_0}{c_2}}, \tag{7.1}$$

where  $c_0, c_1$  and  $c_2$  are defined in (3.5). The second root can be singular, thus here and henceforth, we drop the subscript 2 to simplify notation. A singular point  $(k, \omega) = (k_0, \omega_0)$  can now be defined relative to  $\omega$

$$\omega_0 = \omega(k_0), \quad \omega(k) = \omega_0 + \left. \frac{\partial \omega}{\partial k} \right|_0 (k - k_0) + \frac{1}{2} \left. \frac{\partial^2 \omega}{\partial k^2} \right|_0 (k - k_0)^2 + \dots \tag{7.2}$$

If

$$\left. \frac{\partial \omega}{\partial k} \right|_0 = 0 \text{ at } k = k_0 \quad \text{and} \quad \left. \frac{\partial^2 \omega}{\partial k^2} \right|_0 \neq 0 \text{ at } k = k_0, \tag{7.3}$$

a pinch in the  $k$  plane is a square root branch point in the  $\omega$  plane. We identify  $k_0$  as the roots of

$$\left. \frac{\partial \omega}{\partial k} \right|_{(k_0)} = 0, \quad (k - k_0)^2 = (\omega - \omega_0) / \left[ \frac{1}{2} \left. \frac{\partial^2 \omega}{\partial k^2} \right|_0 \right]. \tag{7.4}$$

The critical singular point satisfies (7.3) and  $\omega_I = 0$ .

Our solution procedure is as follows: the root  $\omega = \omega_R + i\omega_I$ , where  $\omega_R \equiv \omega_R(k_R, k_I)$  and  $\omega_I \equiv \omega_I(k_R, k_I)$ , could be inverted implicitly for

$$k_R = k_R(\omega_R, \omega_I), \quad k_I = k_I(\omega_R, \omega_I). \tag{7.5}$$

The singular point is determined from the condition (7.3). The solutions must be implicit because of the Bessel function. The two real equations in (7.4) may be solved for  $k_R$  and  $k_I$ .

To seek a singular point  $k_0$  at which  $\hat{c} = d\omega/dk = 0$ , the computation is made by means of Newton’s method

$$\hat{c}(k) - \hat{c}(k_s) = \left( \frac{d\hat{c}}{dk} \right)_s (k - k_s), \tag{7.6}$$

where  $k_s$  is a starting value which may be close to the singular point  $k_0$ . Since the solution  $k_0$  is to satisfy  $\hat{c}(k_0) = 0$ , we may rewrite (7.6) as the following iteration algorithm:

$$k = k_s - \hat{c}(k_s) / \left( \frac{d\hat{c}}{dk} \right)_s. \tag{7.7}$$

For given  $k_s$ , the right-hand side of this is calculated to give a next approximate solution  $k$ . The iteration is repeated until  $|k - k_s| < \epsilon$  ( $\epsilon < 10^{-6}$ ) or until the iteration is made over 30 times. The solution  $k_0$  also gives  $\omega(k_0)$ , then we can find the critical singular point when  $\omega_I = 0$ .

### 8. Subcritical, critical and supercritical singular points

The formation and properties of singular points is similar for all cases. Here we shall look at some typical cases for the formation of pinch points in the  $(k_R, k_I)$  plane and cusp points in the  $(\omega_R, \omega_I)$  plane. We use the Weber number parameter  $\beta = \frac{\rho 2aU^2}{\gamma} = W^{-1}$  where  $W$  is the Weber number defined in (2.2).

First we fix the parameters  $(\ell, R, m) = (0, 100, 0)$  and plot lines of constant  $\omega_I$  and  $\omega_R$  in the  $k_R, k_I$  plane in the subcritical ( $\beta = 4.934$ , Fig. 8), critical ( $\beta = 5.134$ , Fig. 9) and supercritical ( $\beta = 5.334$ , Fig. 10) case. The cusp singularity, with  $\omega_I < 0$  at the cusp point is shown in Fig. 11. The pinch point in the subcritical case is in the region  $\omega_I > 0$ ; this is in the region of absolute

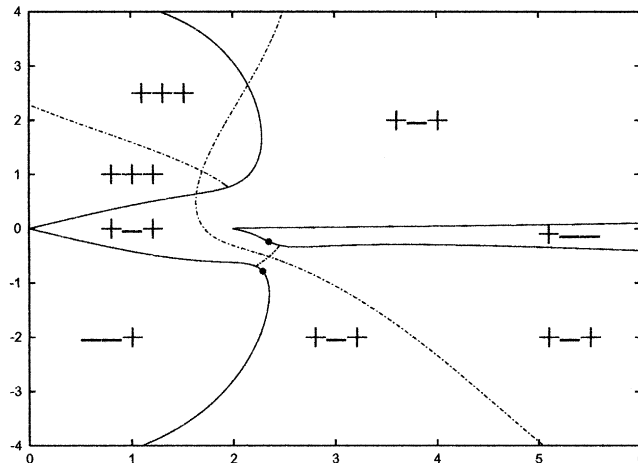


Fig. 8.  $k_I$  versus  $k_R$  for  $\ell = 0, R = 100, \beta = 4.934$ , and  $m = 0$ . Eq. (3.4) gives rise to three complex roots  $k$  for each prescribed set of parameters; for each of the three  $k$ 's there is one value of  $\omega_I$  whose sign is marked on the figure. The value  $\beta = 4.934 < \beta_c = 5.134$  is subcritical. The singular point  $D = 0$  and  $\hat{c} = 0$  (or  $c = \partial\omega_R/\partial k_R = 0$ ) has  $\omega_I > 0$  in the subcritical case and the flow is absolutely unstable; this point is not shown but the points (●) that will merge into a pinch point (●) in Fig. 9 are identified. The solid curves are given by  $D = 0$  and  $\omega_I = 0$ . The dashed curves are for  $D = 0, \omega_R = 1.7178$  and  $\omega_I \geq 0$ .

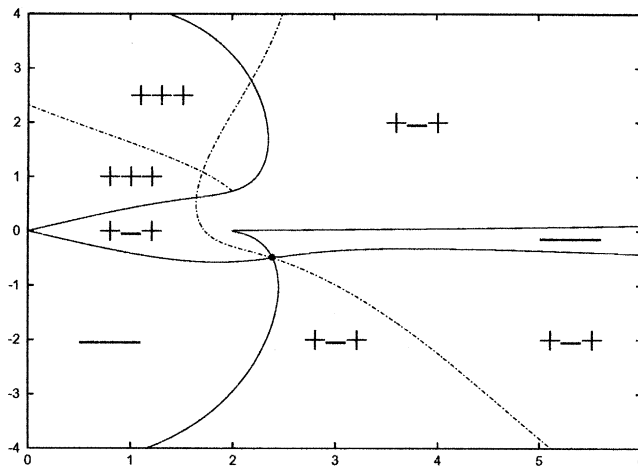


Fig. 9.  $k_I$  versus  $k_R$  for  $\ell = 0, R = 100, m = 0$ , and  $\beta = \beta_c = 5.134$  is critical and identified by (●). At this point  $D = 0, \hat{c} = 0, (\omega_R, \omega_I) = (1.7304, 0)$  and  $(k_R, k_I) = (2.392, -0.496)$ . The dashed curve  $D = 0$  and  $\omega_R = 1.7304$  passes through the critical point and has  $\omega_I \leq 0$ .

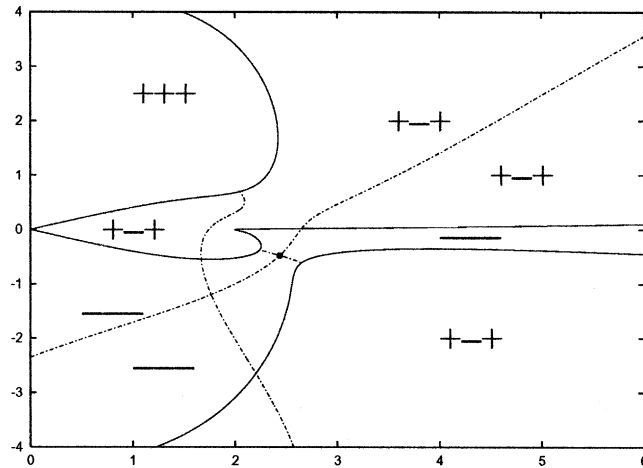


Fig. 10.  $k_I$  versus  $k_R$  for  $\ell = 0$ ,  $R = 100$ ,  $m = 0$ , and  $\beta = 5.334 > \beta_c$  is supercritical. The singular point is shown as a dot (●) and  $\omega_I < 0$  there. On dashed curves  $\omega_R = 1.743$ .

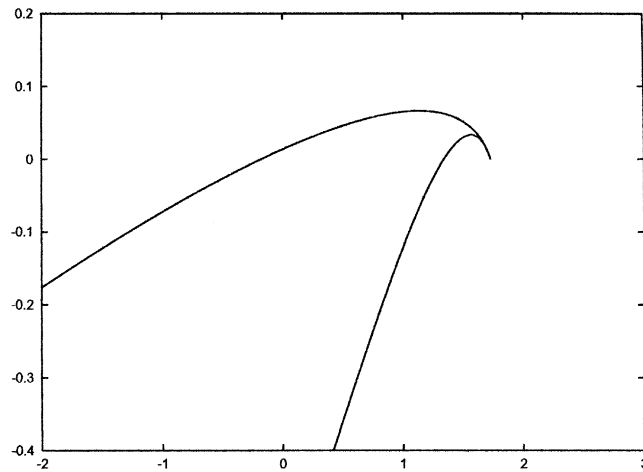


Fig. 11. Cusp point  $(\omega_R, \omega_I) = (1.7304, 0)$ .  $\omega_I$  versus  $\omega_R$  for  $\ell = 0$ ,  $\beta = 5.134$ ,  $R = 100$  and  $m = 0$ ; the solid curves are for  $D = 0$  and  $\hat{c} = 0$ , which passes through the pinch point  $(k_R, k_I) = (2.392, -0.496)$  in the  $(k_R, k_I)$  plane (see Fig. 9).

instability. The pinch point in the supercritical case is in the region  $\omega_I < 0$ ; this is in the region of convective instability.

We draw the reader’s attention to the fact the curves  $k_I(k_R)$  on which  $\omega_R = \text{const}$  typically pass through regions in which  $\omega_I$  is positive and negative. The only curves for which

$$\omega(k_R, k_I(k_R)) = \text{const} \tag{8.1}$$

that lie entirely in regions in which  $\omega_I$  is of one sign pass through the pinch point. In the supercritical case shown in Fig. 10,  $\omega_R = 1.743$  is the only frequency for  $\omega_I < 0$  for all  $k_R$ . Of course, we may interpret  $\omega_R$  as an excitation frequency.

Huerre and Monkewitz (1985) have described the evolution of a wave packet from an impulsive source in the convectively unstable case. They note that

... among all the wavenumbers contained in the impulsive source, the flow selects, along each ray  $x/t = \text{const}$  one particular complex wavenumber  $k^*$  given by

$$\frac{d\omega}{dk}(k^*) = \frac{x}{t}. \tag{8.2}$$

The group velocity then is real and the temporal amplification rate of the wave reduces to

$$\sigma = \omega_I(k^*) - k_I^*(d\omega/dk)(k^*). \tag{8.3}$$

The growth function then becomes

$$\exp(-k_I^*x + \omega_I t) = \exp(\omega_I - k_I^*(d\omega/dk))t. \tag{8.4}$$

Using (6.7) and (6.8), we find that the real part of the group velocity is

$$\frac{\partial\omega}{\partial k}(k^*) = \frac{\partial\omega_R}{\partial k_R}. \tag{8.5}$$

Focusing now on the lines  $\omega_R(k_R, k_I(k_R)) = \text{const}$  in the  $k$  plane (Figs. 8–10) we find that

$$\frac{d\omega_R}{dk_R}(k_R, k_I(k_R)) = \frac{\partial\omega_R}{\partial k_R} + \frac{\partial\omega_R}{\partial k_I} \frac{dk_I}{dk_R} = \frac{\partial\omega_R}{\partial k_R} = 0. \tag{8.6}$$

The only curve  $\omega_R = \text{const}$  which has  $\omega_I \leq 0$  for all  $k_R > 0$  is the one which passes through the pinch point. The harmonic content of the impulsive source produced by this frequency is not restricted. In general the harmonic content of impulsive sources that are convectively unstable depend on the frequency  $\omega_R$  of the excitation.

In the sequel we will describe singular points as points at which the group velocity  $G_V = \partial\omega_R/\partial k_R = 0$ . This is a shorthand for the condition  $D = 0$  and  $\hat{c} = 0$  which is four equations for  $k_R, k_I, \omega_R$  and  $\omega_I$ . All of the graphs shown in the figures to follow satisfy the dispersion relation  $D = 0$ . We have shown in Section 6 that the condition  $\hat{c} = 0$  implies that  $G_V = 0$ . This leads to the condition of Bers (1975) a flow is convectively unstable when  $\omega_I < 0$  and when  $G_V = 0$ .

The qualitative properties of singularities are the same in all cases. At a critical singular point  $\omega_I = 0$ . The values of parameters at critical singular points are given for  $R = 100, 200$  and  $2000$  (Table 3) for three or different values of  $m$  and  $0 \leq \ell \leq 0.4$ . We found that when  $m = 0$ , so that the ambient viscosity is zero, one and only one critical  $\beta$  is found for given values of  $R$  and  $\ell$ . When the ambient viscosity is finite ( $m = 0.5, 1$ ) two critical values are found, but only one is spatially unstable  $k_I < 0$ .

The inviscid case  $R \rightarrow \infty$  is degenerate and will be treated in Section 9.

Figs. 8–10 look at the  $(k_R, k_I)$  plane in the subcritical, critical and supercritical cases for  $(\ell, R, m) = (0, 100, 0)$ . In these figures we plot curves in the  $k_I$  versus  $k_R$  which arise from the real and imaginary part of the dispersion relation  $D(k_R + ik_I, \omega_R + i\omega_I) = 0$  when  $\omega_R$  or  $\omega_I$  is fixed. The singular points are points on the curves which satisfy (6.6). The point in  $(\omega_R, \omega_I)$  plane at criticality is shown in Fig. 11. These graphs are representative for all the nondegenerate cases  $R < \infty$ . The explanations of the figures are given in the captions.

Table 3

Critical values of  $\beta = \beta_c(\ell, R, m)$  at a generic singular point ( $D = 0, \hat{c} = 0$ )

$R$	$m$	$\ell$	$\beta_c$	$k_R$	$k_I$	$\omega_R$	
100	0	0.00	5.134	2.392	-0.496	1.730	
		0.08	5.714	2.550	-0.565	1.823	
		0.16	6.495	2.762	-0.668	1.945	
		0.24	7.596	3.065	-0.834	2.116	
		0.32	9.192	3.510	-1.127	2.360	
		0.40	11.358	4.139	-1.643	2.689	
	1	0.00	13.690	5.899	-1.024	2.585	
		0.08	15.296	6.377	-1.340	2.832	
		0.16	17.452	7.004	-1.830	3.158	
		0.24	20.396	7.837	-2.590	3.589	
		0.32	24.320	8.889	-3.692	4.135	
		0.40	29.182	10.044	-5.129	4.760	
	0.5	0.00	7.206	3.225	-0.309	1.882	
		0.08	8.158	3.478	-0.424	2.026	
		0.16	9.484	3.840	-0.630	2.226	
		0.24	11.352	4.374	-1.010	2.508	
		0.32	13.814	5.129	-1.647	2.879	
		0.40	16.664	6.058	-2.505	3.308	
	200	0	0.00	5.493	2.454	-0.403	1.759
			0.08	6.198	2.646	-0.467	1.868
			0.16	7.193	2.920	-0.569	2.020
0.24			8.696	3.350	-0.753	2.249	
0.32			11.042	4.074	-1.126	2.612	
0.40			14.276	5.203	-1.804	3.131	
1		0.00	13.638	6.046	-0.534	2.612	
		0.08	15.306	6.606	-0.716	2.885	
		0.16	17.720	7.411	-1.036	3.279	
		0.24	21.594	8.698	-1.679	3.906	
		0.32	28.344	10.943	-3.081	4.975	
		0.40	38.728	14.247	-5.688	6.539	
0.5		0.00	7.244	3.238	-0.162	1.891	
		0.08	8.242	3.502	-0.230	2.044	
		0.16	9.694	3.894	-0.374	2.266	
		0.24	11.956	4.565	-0.706	2.616	
		0.32	15.388	5.740	-1.368	3.161	
		0.40	20.154	7.497	-2.412	3.943	
2000		0	0.00	6.065	2.539	-0.192	1.799
			0.08	7.011	2.788	-0.229	1.937
			0.16	8.488	3.191	-0.296	2.151
	0.24		11.154	3.978	-0.447	2.542	
	0.32		16.744	5.865	-0.865	3.417	
	0.40		35.516	12.573	-2.650	6.620	

Table 3 (continued)

$R$	$m$	$\ell$	$\beta_c$	$k_R$	$k_I$	$\omega_R$
1	1	0.00	13.622	6.097	-0.054	2.621
		0.08	15.320	6.690	-0.073	2.905
		0.16	17.868	7.574	-0.109	3.333
		0.24	22.550	9.181	-0.201	4.120
		0.32	38.966	14.774	-0.847	6.873
		0.40	196.642	72.962	-21.449	33.075
0.5	0.5	0.00	7.260	3.242	-0.016	1.894
		0.08	8.274	3.506	-0.024	2.050
		0.16	9.806	3.899	-0.042	2.285
		0.24	12.584	4.610	-0.132	2.713
		0.32	19.602	6.916	-0.665	3.830
		0.40	63.200	22.614	-4.872	11.276

At such a point the group velocity  $\partial\omega_R/\partial k_R = 0$ ,  $(k_R, k_I)$  is a pinch point;  $(\omega_R, \omega_I)$  is a cusp point. A critical singular point also has  $\omega_I = 0$ . When  $\beta < \beta_c$  the flow is subcritical (absolutely unstable) and disturbances with zero group velocity are amplified ( $\omega_I > 0, k_I < 0$ ). When  $\beta > \beta_c$  (convectively unstable) these disturbances decay temporally ( $\omega_I < 0, k_I < 0$ ).

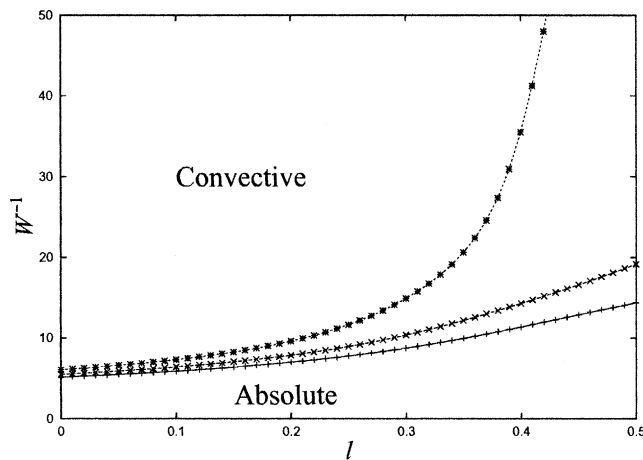


Fig. 12.  $\beta_c$  versus  $\ell$  when  $m = 0.5$ ;  $R = 2000$  (\*),  $200$  (x),  $100$  (+).

In Figs. 12 and 13 we have plotted  $\beta_c$  versus  $\ell$  for  $R = 2000, 200$  and  $100$  when  $m = 0$  and  $m = 0.5$ , respectively.

Fig. 14 gives a summary of the behavior of singular points for inviscid  $R \rightarrow \infty$  and viscous fluids  $R = 100, 200$ . A detailed explanation of this summary in the figure caption.

**9. Inviscid jet in inviscid fluid ( $R \rightarrow \infty, m = 0$ )**

This problem was studied for the case  $\ell = 0$  by Keller et al. (1973); they did not look at the problem of convective/absolute instability—treated later by Leib and Goldstein (1986a). Here

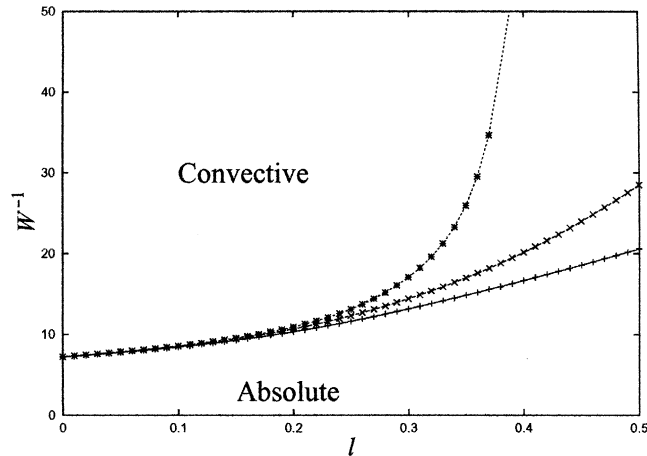


Fig. 13. Gives a summary of the behavior of singular points for inviscid  $R \rightarrow \infty$  and viscous fluids  $R = 100, 200$ . A detailed explanation of this summary is given in the figure caption.

we have looked at the inviscid problem for all density ratios and find the border, the critical  $\beta = \beta_c$  at the singular point (6.2). The singular point is degenerate, because the imaginary part of  $\partial^2 D / \partial k^2$  at the pinch point vanishes for  $0 < \ell < 0.3455$ . The degeneracy appears in the collapse of the region in which  $\omega_I < 0$  for large  $k_R$  into a line; this region of convective instability collapses onto a neutral region for which  $\omega_I = 0$ .

Table 4 lists values of parameter at the pinch point; Fig. 15 gives the critical curve  $\beta_c = \beta(\ell)$  in the  $\beta$  versus  $\ell$  plane.  $\ell = 0.3455$  is an asymptote; when  $\ell > 0.3455$ , there is no pinch point and the flow is absolutely unstable.

**10. Fully viscous flow; comparison with previous results**

Using equations (2.17)–(2.21) in Funada and Joseph (2002) for capillary instability of both viscous fluids, we can modify the dispersion relation (2.17) so as to make the ambient fluid inviscid and the viscous column moving with uniform velocity. The resultant dispersion relation  $D$  for a viscous jet in an inviscid fluid is given by

$$D = \begin{vmatrix} I_1(k/2) & I_1(k_\ell/2) & K_1(k/2) \\ 2k^2 I_1(k/2) & (k^2 + k_\ell^2) I_1(k_\ell/2) & 0 \\ F_1 & F_2 & F_3 \end{vmatrix} = 0, \tag{10.1}$$

where

$$F_1 = (\omega - k)^2 I_0(k/2) + 2i(\omega - k) \frac{k^2}{R} \left( \frac{dI_1(k/2)}{d(k/2)} \right) + W(4 - k^2) k I_1(k/2), \tag{10.2}$$

$$F_2 = 2i(\omega - k) \frac{k k_\ell}{R} \left( \frac{dI_1(k_\ell/2)}{d(k_\ell/2)} \right) + W(4 - k^2) k I_1(k_\ell/2), \tag{10.3}$$

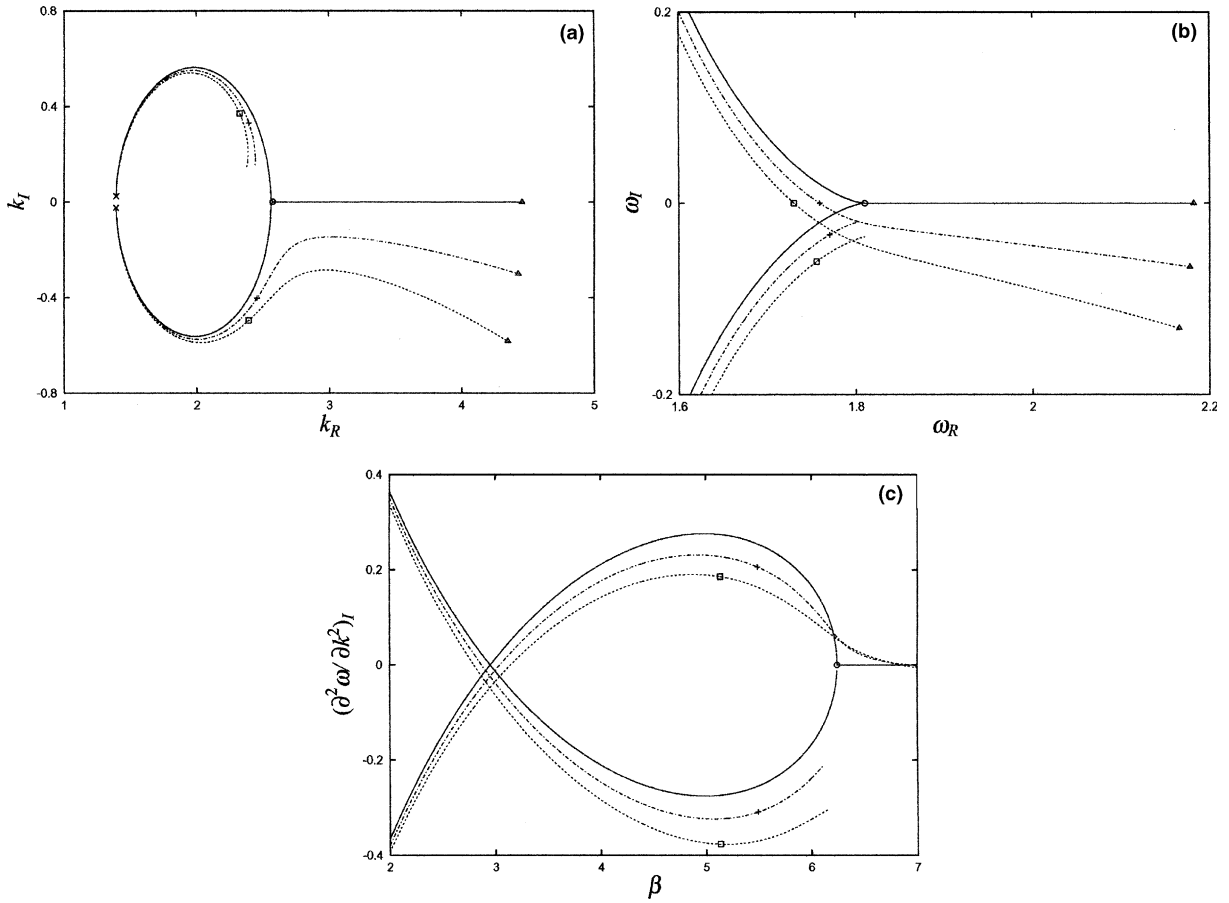


Fig. 14. Locus of singular points  $D = 0, \hat{c} = 0$  for  $m = 0, \ell = 0, R = 100$  (dashed line),  $R = 200$  (dash dot line),  $R \rightarrow \infty$  (solid line) for  $10^{-3} \leq \beta \leq 10$ . Critical singular points are those for which  $\omega_I = 0$ .  $\beta = 10^{-3}$  ( $\times$ ),  $\beta \hat{c} = 6.246$  ( $\circ$ )  $\hat{c} \beta_c = 5.134$  ( $\square$ ),  $\beta_c = 5.493$  ( $+$ ) and  $\beta = 10$  ( $\triangle$ ). (a)  $k_I$  versus  $k_R$ , (b)  $\omega_I$  versus  $\omega_R$ , (c)  $(\partial^2 \omega / \partial k^2)_I$  versus  $\beta$ .  $\beta < \beta_c$  is subcritical,  $\beta > \beta_c > 0$  is supercritical. The supercritical inviscid branch  $R \rightarrow \infty, \beta > 6.246$  is degenerate  $(\partial^2 \omega / \partial k^2)_I = \omega_I = k_I = 0$  there. Disturbances with zero group velocity are neutrally stable. The values of  $\beta$  on the upper branches  $k_I > 0$  of the  $(k_R, k_I)$  plane are less than  $\beta_c = 6.246$  and  $\omega_I < 0$ . These branches are subcritical and spatially and temporally damped. The lower branches  $k_I < 0$  go from subcritical values  $10^{-3} < \beta < \beta_c$  for  $\omega_I > 0$  (for which the disturbances are spatially and temporally amplified) to supercritical values  $\beta > \beta_c$ :  $\beta_c = 6.246$  for  $R \rightarrow \infty$  and  $\omega_I = 0, k_I = 0$  for  $\beta > 6.246, \beta_c = 5.134$  for  $R = 200$  and  $\omega_I < 0$  there,  $\beta_c = 5.493$  for  $R = 100$  and  $\omega_I < 0$  there. Disturbances with zero group velocity are temporally damped but spatially amplified ( $\omega_I < 0, k_I < 0$ ) for supercritical values of  $\beta$ .

$$F_3 = -\ell \omega^2 K_0(k/2), \tag{10.4}$$

with  $k_\ell$  defined as

$$k_\ell = \sqrt{k^2 - iR(\omega - k)}. \tag{10.5}$$

Table 4  
Inviscid fluids ( $R \rightarrow \infty, m = 0$ )

No.	$\ell$	$\beta_c$	$k_R$	$k_I$	$\omega_R$	$\omega_I$
1	0.00	6.246	2.576	0	1.810	0
2	0.04	6.710	2.696	0	1.877	0
3	0.08	7.280	2.840	0	1.958	0
4	0.12	8.004	3.025	0	2.060	0
5	0.16	8.962	3.290	0	2.196	0
6	0.20	10.298	3.681	0	2.387	0
7	0.24	12.282	4.274	0	2.677	0
8	0.28	15.496	5.317	0	3.162	0
9	0.32	22.038	7.514	0	4.199	0
10	0.3455	52.350	17.647	0	9.189	0
11	0.36	—	—	—	—	—
12	0.40	—	—	—	—	—

Values of  $(k_R, k_I)$  at pinch point singularity (see Fig. 15) indexed by the density ratio  $\ell$ . The values of the frequency  $\omega_R$  and the Weber number parameter  $\beta (=W^{-1})$  are at the pinch point are also listed. Pinch point singularities do not exist when  $\ell > 0.3455$ ; in this case all flows are absolutely unstable.

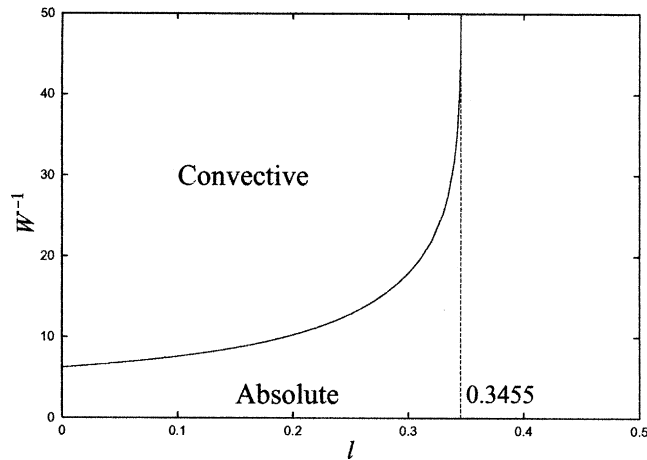


Fig. 15. Border between absolute and convective instability in the inviscid case  $R \rightarrow \infty, m = 0$ . The value of  $\ell = 0.3455$  is asymptotic. The inviscid case is degenerate because the imaginary part of  $\partial^2\omega/\partial k^2 = 0$  at the singular point. The consequence of this degeneracy is that at criticality  $(\omega_I, k_I) = (0, 0)$  for all  $\ell < 0.3455$ . The condition  $\omega_I < 0$  at the pinch point cannot be realized;  $\omega_I$  at  $\partial\omega_R/\partial k_R = 0$ .

The parameters  $\ell, W$  and  $R$  are the ones defined in (2.2). The top row of (10.1) arises from the continuity of normal velocity, of the tangential stress and of the normal stress. Solving (10.1) implicitly using Newton’s method for given values of  $(\omega_R, \omega_I)$  and the parameters, we have  $(k_R, k_I)$  and  $\hat{c}$  numerically.

In Fig. 16 we have plotted the critical value  $\beta_c (=W_c^{-1})$  versus  $R$  giving the border between absolute and convective instability for viscous jets in an inviscid fluid computed by Leib and

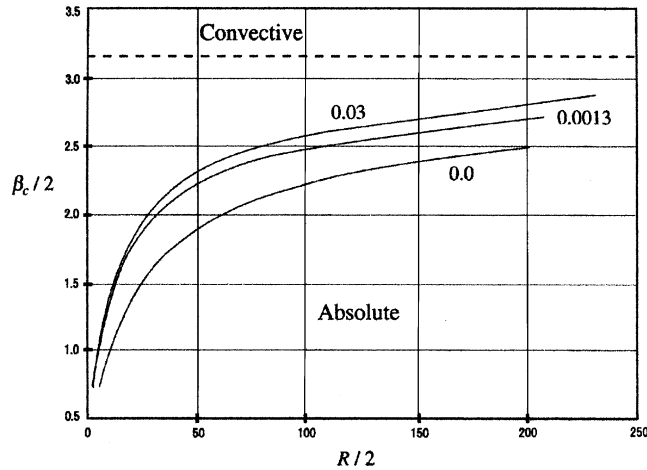


Fig. 16. Critical Weber number  $\beta_c$  ( $= W_c^{-1}$ ) versus Reynolds number  $R$  from the literature: Leib and Goldstein (1986a) for inviscid jet in an inviscid fluid,  $\beta_c = 6.3$  for  $\ell = 0$ , denoted by dashed line; solid lines are for viscous jets in an inviscid fluid ( $m = 0$ ) for  $\ell = 0$  (Leib and Goldstein, 1986b) and  $\ell = 0.0013$  and  $\ell = 0.03$  (Lin and Lian, 1989).

Goldstein (1986b) for  $\ell = 0$  and by Lin and Lian (1989) for  $\ell = 0.0013$  and  $\ell = 0.03$ . The value  $\beta_c = 6.3$  for an inviscid jet in an inviscid fluid was calculated by Leib and Goldstein (1986a). In Fig. 17 we compare the results from the theory of viscous potential flow given in Section 3 with the results for viscous flow according to (10.1). The stability limits from the two theories are close.

The analysis for “fully viscous flow” neglects the dynamical effects of the viscous gas; these effects require the imposition of continuity of the tangential component of velocity and stress. The discontinuous velocity which induces Kelvin–Helmholtz instability is then inconsistent with the aforementioned continuity requirements. Lin (2003) attempted to address the effects of shear

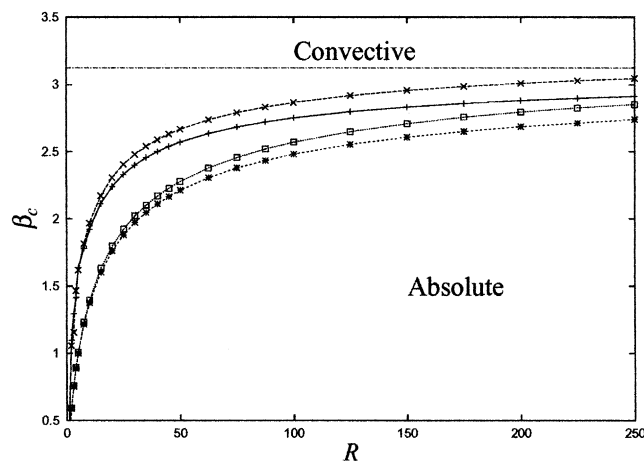


Fig. 17.  $\beta_c$  versus  $R$  comparing viscous flow (lower two curves) computed from the theory in Section 10 for  $m = 0$ ,  $\ell = 0.0013$  (\*) and  $\ell = 0.03$  (□) with viscous potential flow (upper two curves) for the same values ( $\ell = 0.0013$  (+),  $\ell = 0.03$  (×),  $m = 0$ ).

by a study of core-annular flow in a vertical pipe. This is a very different problem. He found a transition from convective to absolute instability but comparisons with experiments are not available.

## 11. Conclusions

The new results presented in this paper are:

- (1) The computation of temporal and C/A instability of the liquid jet using viscous potential flow.
- (2) Extensive computation of the effects of the ambient density and viscosity and the viscosity of the liquid.
- (3) A demonstration that KH instability cannot occur in vacuum (but capillary instability and Rayleigh–Taylor instability can occur in vacuum).
- (4) The derivation of a dispersion relation in the form of a polynomial in the complex frequency which can be used to study temporal, spatial and C/A instability.
- (5) A comprehensive analysis of temporal instability; for all values of the parameters there are wavenumbers for which the liquid jet is unstable.
- (6) An analysis of the relative importance of KH and capillary instability on the maximum growth, on the wave length of maximum growth and the cut-off wavenumber for inviscid and viscous liquids. KH instability is the dominant mechanism for small Weber numbers and capillary instability is dominant for large Weber numbers; the variation of the growth rates and wavenumbers in the two regimes is sharply different.
- (7) When viscosity and surface tension are zero, the liquid jet is Hadamard unstable to KH instability with growth rates proportional to  $k$ . Surface tension stabilizes the short waves. The maximum growth rate and the associated wavenumber are proportional to  $1/W$  for small  $W$  when the fluid is inviscid. For viscous fluids the maximum growth rate is finite as  $W \rightarrow 0$  (pure KH instability) but the wave length  $\lambda_m = 2\pi/k_m$  tends to zero with  $W$ , as in the inviscid case. It can be said that the wave lengths for breakup due to KH instability are exceedingly short and that breakup due to KH instability leads to surpassingly small drops, essentially mist.
- (8) The critical wavenumber  $k_c$  for marginal instability (stability for  $k > k_c$ ) is independent of the Reynolds number of the liquid jet but the maximum growth rate and the wavenumber of maximum growth depend on the Reynolds number.
- (9) Under the realizable condition that  $ma b_a = \ell b \alpha_a$  the neutral curves for viscous potential flow are the same as for inviscid potential flow; this is a remarkable result. When  $k > 10$  this criterion reduces to a statement that the neutral curves are the same when the kinematic viscosity of the liquid equals the kinematic viscosity of the gas; this result was proved for KH instability of a plane layer by Funada and Joseph (2001).
- (10) A comprehensive study of the transition between convective and absolute stability of the combined KH stability and capillary instability of the liquid jet under a wide range of ambient condition for different liquid was carried out. Precise results were obtained for full ranges of the Weber and Reynolds number, density and viscosity ratios.

- (11) The study of pinch point and cusp point singularities was greatly simplified by the fact that an explicit dispersion relation in the complex frequency and wavenumber planes could be studied by algebraic rather than geometric method of Bers (1975) and Briggs (1964).
- (12) We show that the singular point for inviscid fluids when the density ratio  $\ell$  is in  $0 \leq \ell < 0.3455$ , is degenerate; when  $\ell > 0.3455$  the inviscid jet is absolutely unstable. The singular points for inviscid solutions in the supercritical case  $\beta > \beta_c$  are degenerate since  $(\partial^2 \omega / \partial k^2)_I = 0$ . In this case  $k_I = 0$  and  $\omega_I = 0$ , so that the transition from absolute instability is to a neutral rather than to a convectively unstable state. All other cases are not degenerate and associate cusp points in the  $\omega$  plane with pinch points in the  $k$  plane.
- (13) The transition between convective and absolute stability computed by viscous potential flow is reasonably good agreement with the transition computed by fully viscous flow in which the flow is not assumed to be irrotational. It must be understood that KH instability cannot be studied exactly in the frame of the Navier–Stokes equations because the basic flow has a discontinuous velocity.

The liquid jet with no spatial development studied here is always unstable to temporal disturbances, convectively and absolutely unstable jets are temporally unstable; flows like Hagen–Poiseuille flow which are temporally stable would not admit C/A instability. Instability for jets with very slow spatial development should not be very different for jets with no spatial development. The predictions of temporal and C/A instability achieved here have a somewhat tentative relation to actual experiments which emanate from nozzles in which the spatial development of the basic flow could have an important effect.

### Acknowledgment

This work was supported by the NSF/CTS-0076648, the Engineering Research Program of the Office of Basic Energy Sciences at the DOE.

### References

- Bers, A., 1975. Linear waves and instabilities. In: DeWitt, C., Peyraud, J. (Eds.), *Physique des Plasmas*. Gordon and Breach, New York, pp. 117–213.
- Briggs, R.J., 1964. Electron-stream interaction with plasmas Research Monograph, 29. MIT Press, Cambridge, Mass.
- Drazin, P.G., Reid, W.H., 1981. *Hydrodynamic Stability*. Cambridge University Press.
- Funada, T., Joseph, D.D., 2001. Viscous potential flow analysis of Kelvin–Helmholtz instability in a channel. *J. Fluid Mech.* 445, 263–283.
- Funada, T., Joseph, D.D., 2002. Viscous potential flow analysis of capillary instability. *Int. J. Multiphase Flow* 28, 1459–1478.
- Huerre, P., 2000. Open shear flow instabilities. In: Batchelor, G.K., Moffatt, H.K., Worster, M.G. (Eds.), *Perspectives in Fluid Dynamics*. Cambridge University Press, pp. 159–229.
- Huerre, P., Monkewitz, P.A., 1985. Absolute and convective instabilities in free shear layers. *J. Fluid Mech.* 159, 151–168.
- Joseph, D.D., 1990. *Fluid Dynamics of Viscoelastic Flows*. Springer-Verlag.
- Joseph, D.D., Liao, T.Y., 1994. Potential flows of viscous and viscoelastic fluids. *J. Fluid Mech.* 265, 1–23.

- Joseph, D.D., Saut, J.C., 1990. Short-wave instabilities and ill-posed initial-value problems. *Theor. Comp. Fluid Dyn.* 1, 191–227.
- Keller, J.B., Rubinow, S.I., Tu, Y.O., 1973. Spatial instability of a jet. *Phys. Fluids* 16, 2052–2055.
- Le Dizès, S., 1997. Global modes in falling capillary jets. *Eur. J. Mech. B/Fluids* 16, 761–778.
- Leib, S.J., Goldstein, M.E., 1986a. The generation of capillary instability on a liquid jet. *J. Fluid Mech.* 168, 479–500.
- Leib, S.J., Goldstein, M.E., 1986b. Convective and absolute instability of a viscous liquid jet. *Phys. Fluids* 29, 952–954.
- Li, H.-S., Kelly, R.E., 1992. The instability of a liquid jet in a compressible airstream. *Phys. Fluids A* 4, 2162–2168.
- Lin, S.P., 2003. *Breakup of Liquid Sheets and Jets*. Cambridge University Press.
- Lin, S.P., Lian, Z.W., 1989. Absolute instability in a gas. *Phys. Fluids A* 1, 490–493.
- Mata, C., Pereyra, E., Trallero, J.L., Joseph, D.D., 2002. Stability of stratified gas–liquid flows. *Int. J. Multiphase Flow* 28, 1249–1268.
- Rayleigh, L., 1878. On the instability of jets. *Proc. Lond. Math. Soc.* 10, 4–13.
- Schmid, P., Henningson, D.S., 2001. *Stability and Transition in Shear Flows*. Springer-Verlag.
- Yang, H.Q., 1992. Asymmetric instability of a liquid jet. *Phys. Fluids A* 4, 681–689.